Faculty of Science and Engineering

Western Australian School of Mines

Assessing the Condition of Rock Tools through Waveform Analysis Techniques of Rock Drilling Induced Vibration Signals

Don Sameera Wishwajith Hettiarachchi

This thesis is presented for the Degree of
Master of Philosophy (Mining Engineering)
of
Curtin University

June 2016

PUBLICATIONS INCORPORATED INTO THIS THESIS

Hettiarachchi D. S., Kawamura Y., Takarada Y., Karakus M., Jang H.D., 2016. A case study of assessing button bit failure through Wavelet Transform using rock drilling induced noise signals, *Journal of Tunnelling and Underground Space Technology* (under review)

ACKNOWLEDGEMENTS

I would like to express my sincere gratitude to my previous supervisor Professor Youhei Kawamura, for giving me the opportunity to pursue my higher education under his excellent supervision and guiding me throughout this period.

I would also wish to express my gratitude to my current supervisor Dr. Oktay Erten and my co-supervisor Dr. Hyong Doo Jang for their valuable support in completion of my studies.

I want to gratefully acknowledge Mitsubishi Materials Corporation and the Mining Company, especially Mr. Yusuke Takarada for the support given to me throughout the data collection process.

A special thank goes to Dr. Mahinda Kuruppu for coordinating my enrolment in the Mphil degree at WA School of Mines, Curtin university and all the academic staff at WA School of Mines for the support given throughout my research period.

I would also like to thank my colleagues, Dr. D. S. S. Sandanayake and Mr. Ushan de Zoysa for their encouragement during my studies.

Finally, I would like to give my sincere appreciation to my parents, my wife and my sister for being with me and encouraging me throughout my studies.

ABSTRACT

Drilling is one of the most important processes in hard rock mining. With the rapid fluctuations of the commodity prices, it is vital to gain the maximum recovery with the minimum extraction cost at all the time. Due to the heavy influence of hard rock drilling towards the extraction of minerals, even a slight increase in productivity in hard rock drilling can lead to a substantial increase in profits for the company. Hence, the recognition of the optimum drilling conditions will assist to minimise the extraction costs as well as to increase the productivity, which will eventually aid to increase the profits of the company.

Since tapered button bits can be used in wide range of rock types, they are predominantly adopted in production drilling in mining industry. It is vital to detect the precise moment of button failure of a drill bit during a real time drilling process because a failure of a button can significantly increase the potential to destroy all other buttons and drop the penetration rate. Thus, it is vital to detect the exact moment of button failure to avoid the further damage to the buttons and to maintain a reasonable penetration rate.

Over the years, the detection of button failure depends on the empirical intuition of drill rig operators. However, with the complexity of a real time drilling process, it is susceptible to errors and not reliable. This research introduces a new methodology to detect the exact moment of button failure of drill bit during a real time drilling process.

The experiment was conducted in an underground mine in Queensland, Australia, in collaboration with Mitsubishi Materials Corporation. Video and sound data were recorded during a real time drilling process, which used 45 mm diameter of Poly Crystalline Diamond (PCD) tapered button bits to drill 4 m holes in to brecciated granite hard rock. The recorded frantic sound signal was analysed using different signal processing techniques, including, Time series, Fourier Transform and Wavelet Transform analysis.

The results of this research clearly indicates that the exact moment of button failure of a drill bit during a real time drilling process can be identify by analysing the sound of drilling process with Wavelet Transform. Moreover, it demonstrates that the Wavelet Transform is a more effective waveform analysis technique to detect the singularity

points such as button failures, in comparison to Time series analysis and Fourier Transform.

TABLE OF CONTENTS

LIST OF FIGURES

LIST OF TABLES

CHAPTER 1. INTRODUCTION

Hard rock drilling plays a pivotal role among the mining operations that guides the extraction of valuable minerals. The efficiency in drilling aids to the smooth flow of operations in mining industry. Even a small increase in efficiency in had rock drilling can lead to a considerable cost savings. A rapid and accurate detection of abnormalities in drilling tools will aid to increase the efficiency in hard rock drilling. Thus, it is vital to identify the drilling tool conditions for prime performance of any drilling operation.

Tapered button bits are mainly used for production rotary drilling and it is very popular in modern mining industry since, it can be used for the rock types which has a uniaxial compressive strength of 80 MPa to 200 MPa ("Mitsubishi Rock Tools,"). In rotary drilling rock fragmentation mechanism is a complex process which comprises of one or numerous cutting processes such as indentation, grinding, shearing, ploughing, cutting and crushing (Barry et al., 1992; Paone & Bruce, 1963; Paone et al., 1966; Rowlands, 1974). However, a combination of horizontal torque force (Torque on the bit) and vertical thrust force (weight on the bit) imposing to the rock by drill bit contributes more towards the rock fragmentation (K. Rao et al., 2002). Weight on the bit plays a major role on penetration rate as well as the wearing of bits rather than the torque on the bit (Huang & Wang, 1997).

Crushing down and chipping of buttons, cracking the carbide and button shearing off to the level of the body are some common forms of unwanted button failures, which occurred mainly due to over wearing of bits and drilling in to the metal particles which are broken from the drill bit itself. For instance, button failure caused by drilling in to metals, will eventually affect to damages of the other buttons of the bit. Hence, it is vital to identify the exact initial moment of failure of the button of a drill bit.

The drilling process always generates noise which is usually emitted at the interface of drill bit and the drilling surface. The characteristics of the noise depends on the physical properties of the material of the drill bit and the drilling surface. For example, sound generated by a small household drill boring in to a wood is different to the sound created by the same drill boring in to a metal and both those sounds are entirely different to the sound generated by a hard rock drilling process. Few researches have been done to identify the noise characteristics of drill bits in hard rock drilling (Gradl et al., 2011; Karakus & Perez, 2014). However, no researches have been conducted to

develop a method to identify the precise moment button failure of a drill bit in hard rock drilling. Thus, an introduction of a reliable method to detect the exact moment of button failure of a drill bit will aid to optimise the profits of mining operations.

1.1 Statement of Problem

The price of the mineral commodities has been fluctuating rapidly with the changes of demand for those minerals. Thus it is vital to get the maximum recovery with the minimum extraction costs at all times. The heavy influence of hard rock drilling towards the extraction of minerals makes it important to optimise the drilling to minimise the costs.

The difficulty of detecting the precise moment of button failures of drill bits during a hard rock drilling process is a main issue in mining industry. If one button breaks during a drilling process, it tends to create failures of the other buttons of the same bit. Furthermore, a button failure of a drill bit decreases the penetration rate of drilling, which will reduce the mine production rates as well as increase of rig operator hours. Thus, to avoid further damage to the buttons of the drill bit and to maintain a balanced production rate with minimum cost, it is crucial for the operator to identify the precise moment of the button failure, which will ultimately benefit to the yield of the company.

Over the years, detecting the defects in drilling tool conditions such as over wear and button failures, solely depend on the experience of the drill rig operators, which is subjective and susceptible to human errors. Thus, a reliable method to detect the abnormalities in drilling tool conditions is one of the major requirement of the modern vibrant mining industry, which is constantly pursuing techniques to optimise the production with a minimum cost.

A reliable method have not been introduced to detect the button failures of drill bits in hard rock drilling. The aim of this research is to introduce a reliable method to detect the precise moment of button failure of a drill bit. The proposed methodology will be beneficial to mining industry to minimise the cost of production by reducing the cost on drilling tools and by maintaining a healthy penetration rate while drilling.

1.2 Research Aims and Objectives

The objectives of this research are;

- Review the existing methods of tool condition monitoring to identify the ways to incorporate those methods to detect the failure of button in drill bits.
- Review the previous researches to assess the effectiveness of data types (Sound, Vibration) that can be used for the analysis.
- Develop a research methodology to collect the required data.
- Analyse the data using waveform analysis techniques to find the precise moment of button failure by utilizing the available software (OriginPro and Geo-Lab Analyser).
- Statistical analyse of data to sustenance the findings of the Waveform analysis method.

1.3 Outline of Thesis

Chapter 1 presents an introduction about sound generated by hard rock drilling and the problem statement. Furthermore, it explains the research objectives and the importance of this project to the modern mining industry.

Chapter 2 explains the different signal processing techniques and the theories used in this research to achieve the objectives. It includes an overview of Fourier series theory and a detailed description of Wavelet transform theory. This chapter also describes about the different Wavelet transform methods and its uses.

Chapter 3 presents the literature review of the previously conducted researches in related to the sound generated by rock bit interactions and the use of waveform analysis techniques in the study area of tool condition monitoring. This chapter also includes reviews of the studies of different monitoring techniques in tool condition monitoring and machine dynamics.

Chapter 4 describes the methodology of the research. This includes a brief description about the location which the test was conducted and the arrangement of the apparatus to gather the data. This chapter also explains the general experimental procedure, which consist of the data collection and data preparation procedures for the analysis.

Chapter 5 explains the detailed data analysis procedure, which includes the video data analysis and sound data analysis to detect the precise time of button failure of the drill

bit. This also describes the statistical analysis procedure which correlates the findings of waveform analysis techniques and the analysis of real time penetration rates.

Chapter 6 presents the overall test results and discussion. This chapter explains the results of different waveform analysis techniques, which are time series analysis, FFT analysis and Wavelet transform. Furthermore, it describes the results of statistical analysis and real time penetration rate analysis and how those results can be correlated to the results of waveform analysis techniques.

Chapter 7 presents the summary of outcomes of the research and provides recommendations for further research developments in the study area.

1.4 Summary

Detecting the exact moment of button failure of a drill bit during a real time hard rock drilling process will aid to optimise the efficiency of drilling operations. Using the experience of drill rig operators to identify the exact moment of button failure is not reliable. This research introduces a reliable method to identify the exact moment of button failure of a drill bit.

CHAPTER 2. SIGNAL PROCESSING TECHNIQUES

2.1 Introduction

This chapter mainly overviews the theories associated with different signal processing techniques, which have been reviewed and used during this research project. Fourier Transform and Wavelet Transform are two main signal processing techniques which are in use over the years in tool condition monitoring. Discrete Fourier transform and Fast Fourier Transform have been used to analyse the frequency spectrum of a time domain signal. Continuous Wavelet Transform and Discrete Wavelet Transform are two main wavelet techniques which have been used in time – frequency analysis of a time domain signal.

2.2 Fourier Series and Fourier Transform

Fourier series was first introduced by Joseph Fourier with the idea of expansion of a function in terms of trigonometric series. Fourier series and Fourier transform is been considered as one of the best discoveries in mathematics and widely use in different applications in physics, mathematics and engineering (Shah, 2015).

The Fourier series of a function $f(x)$on the interval of $(-l,\ l)$ defined as:

$$f(x) = \sum_{n=-\infty}^{\infty} c_n e^{\frac{in\pi x}{l}} \tag{1}$$

Where c_n is the Fourier coefficient and can be defined as;

$$c_n = \frac{1}{2l} \int_{-\infty}^{\infty} f(t)\, e^{\frac{-in\pi x}{l}} \tag{2}$$

The Fourier integral theorem has been formulated by taking the limit $l \to \infty$ and it is represented for a non-periodic function for all real x, as follows:

$$f(x) = \frac{1}{2\pi} \int_{-\infty}^{\infty} e^{i\omega x}\ d\omega \int_{-\infty}^{\infty} e^{-i\omega t}\ f(t)dt \tag{3}$$

Fourier transform was invented from the Fourier integral theorem and the Fourier transform of a signal $f(t)$ is defined as:

$$\hat{f}(\omega) = \int_{-\infty}^{\infty} e^{-i\omega t}\ f(t)dt \tag{4}$$

Where $\hat{f}(\omega)$ is the Fourier transform of the signal $f(t)$, ω is the frequency and the notation $e^{-i\omega t}$ is called the Euler's equation which is defined as follows:

$$e^{i\omega t} = \sin \omega t + i \cos \omega t \tag{5}$$

Fourier inverse formula can reinstate the signal $f(t)$ from its Fourier transform $\hat{f}(\omega)$ for certain conditions, which makes the Fourier transform technique successful in analysing harmonic signals. The Fourier inverse formula is defined as:

$$f(t) = \frac{1}{2\pi} \int_{-\infty}^{\infty} e^{i\omega t}\ \hat{f}(\omega)d\omega \tag{6}$$

2.2.1 Discrete Fourier Transform

Fourier transform was developed to calculate the frequency spectrum of a continuous signal, which is at all values of time. However, in most of the applications, continuous signals are sampled at different time intervals. Thus, the Fourier transform is not able to calculate the coefficients accurately for those discrete signals. Discrete Fourier Transform has been introduced to overcome the difficulties of Fourier transform and it is identical to the Fourier transform for the signals sampled at finite sample points.

Consider the Fourier transform of the signal f.

$$\hat{f}(\omega) = \int_{-\infty}^{\infty} e^{-i\omega t}\ f(t)dt \tag{7}$$

Let the N sample points be $f[0], f[1], f[2], \dots, f[k], \dots, f[N-1]$.

$$\hat{f}(\omega) = \int_{0}^{(N-1)T} e^{-i\omega t}\ f(t)dt \tag{8}$$

$$\hat{f}(\omega) = f[0]e^{-i0} + f[1]e^{-i\omega T} + f[2]e^{-i\omega 2T} + \cdots + f[k]e^{-i\omega kT} + \cdots + f[N-1]e^{-i\omega(N-1)T} \tag{9}$$

$$\hat{f}(\omega) = \sum_{k=0}^{N-1} f[k]\, e^{-i\omega kT} \tag{10}$$

Discrete Fourier Transform considered the finite number of sampled points as if it were periodic. For instance, the layout of the signal from 0 to (N-1) points is the same as the N to (2N-1). Figure 1 shows an example of the harmonic discrete signal. The graph on the top illustrates the one period of a harmonic signal displays on the graph on the bottom.

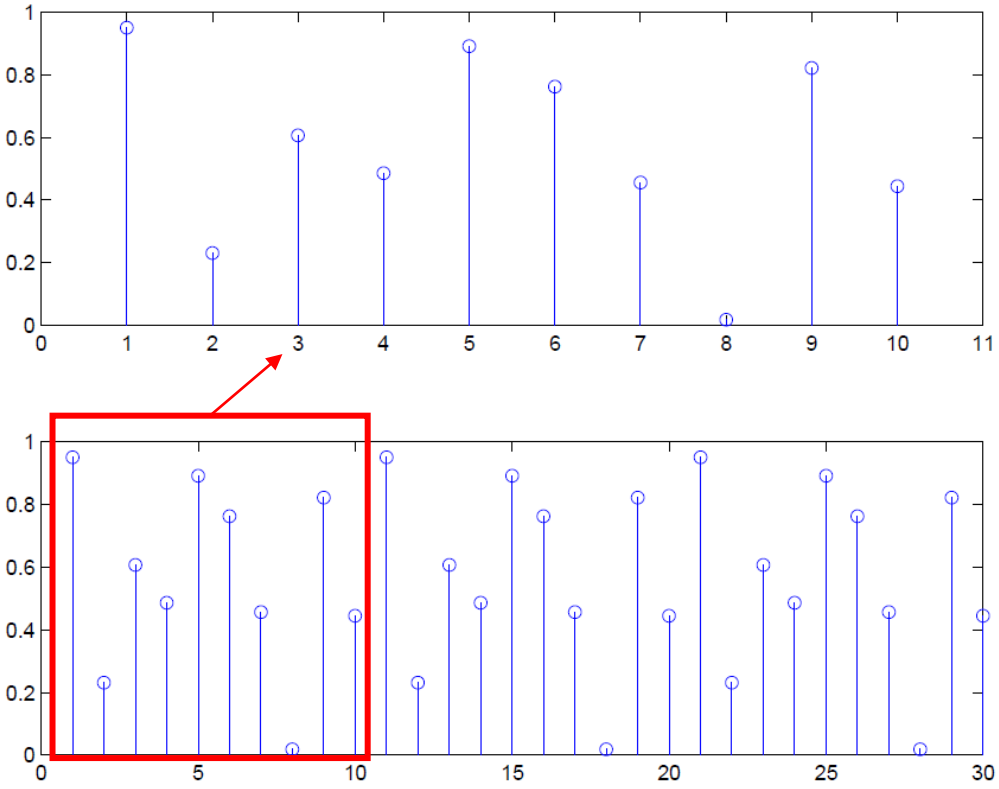

Figure 1: Example of a discrete harmonic signal - One period (Top) and the total discrete signal (Bottom)

The Discrete Fourier Transform has been constructed for the fundamental frequency and its harmonics, as the technique considers the data as periodic.

Thus, in general Discrete Fourier Transform $[f(n)]$ of the series $f(k)$ can be defined as:

$$\hat{f}(n) = \sum_{k=0}^{N-1} f[k] e^{-ink\frac{2\pi}{N}} \qquad (n = 0 : N-1) \tag{11}$$

Where $\omega = 0, \frac{2\pi}{NT}, \frac{2\pi}{NT} \times 2, \dots, \frac{2\pi}{NT} \times n, \dots, \frac{2\pi}{NT} \times (N-1)$.

The Discrete Fourier Transform equation can be represented in a matrix as follows:

$$\begin{bmatrix} \hat{f}\,(0) \\ \hat{f}\,(1) \\ \hat{f}\,(2) \\ \vdots \\ \hat{f}\,(N-2) \\ \hat{f}\,(N-1) \end{bmatrix} = \begin{bmatrix} 1 & 1 & 1 & 1 & \vdots & 1 \\ 1 & W & W^2 & W^3 & \vdots & W^{N-1} \\ 1 & W^2 & W^4 & W^6 & \vdots & W^{N-2} \\ 1 & W^3 & W^6 & W^9 & \vdots & W^{N-3} \\ \vdots & \vdots & \vdots & \vdots & \vdots & \vdots \\ 1 & W^{N-1} & W^{N-2} & W^{N-3} & \vdots & W \end{bmatrix} \begin{bmatrix} f(0) \\ f(1) \\ f(2) \\ \vdots \\ f(N-1) \end{bmatrix} \tag{12}$$

Where $W = (e^{-i\frac{2\pi}{N}})^{2N}$.

2.2.2 Fast Fourier Transform

The number of calculations required to find the frequency components of a signal by using the Discrete Fourier Transform is enormous. Thus, a much simplified calculation to evaluate the Discrete Fourier Transform was required to use the technique in practical applications. Cooley and Tukey (1965), discovered a numerical algorithm to evaluate the Discrete Fourier Transform with a significantly less amount of calculations, which is called as Fast Fourier Transform. The introduction of the digital computer and the new algorithm created the path to acquire the Discrete Fourier transform of a signal quickly and accurately (Shah, 2015).

Consider the Discrete Fourier Transform equation:

$$\hat{f}(n) = \sum_{k=0}^{N-1} f[k] e^{-ink\frac{2\pi}{N}} \tag{13}$$

$$\hat{f}(n) = \sum_{k=0}^{N-1} f[k] W_N^{nk} \tag{14}$$

Where, $W_N = e^{-2i\frac{\pi}{N}}$.

By dividing the equation of Discrete Fourier Transform of f in to the two, that is one for the even parts and the other for the odd parts, the following equations can be obtain.

$$\hat{f}(n) = \sum_{m=0}^{\frac{N}{2}-1} f[2m]\, W_N^{2mn} + \sum_{m=0}^{\frac{N}{2}-1} f[2m+1]\, W_N^{(2m+1)n} \tag{15}$$

Where $m = \frac{k}{2}$ for even parts and $m = \frac{k-1}{2}$ for odd parts. Furthermore,

$$W_N^{2mn} = e^{-i(2mn)\frac{2\pi}{N}} = e^{-imn\frac{2\pi}{\frac{N}{2}}} = W_{\frac{N}{2}}^{mn} \tag{16}$$

Therefore,

$$\hat{f}(n) = \sum_{m=0}^{\frac{N}{2}-1} f[2m]\, W_{\frac{N}{2}}^{mn} + W_N^m \sum_{m=0}^{\frac{N}{2}-1} f[2m+1]\, W_{\frac{N}{2}}^{mn} \tag{17}$$

$$\hat{f}(n) = g[n] + W_N^m h[n] \tag{18}$$

The Discrete Fourier Transform, $\hat{f}(n)$, of N samples can be achieved by dividing the N number of points into two $\frac{N}{2}$ points and obtaining one Discrete Fourier Transform for even data ($g[n]$) and another transform for the odd data ($h[n]$).

For a N times sampled signal, Discrete Fourier Transform requires N^2 multiplications in comparison to the $N \log_2 N$ multiplications for the same signal, with the Fast Fourier Transform calculations (Shah, 2015). For instance, a signal with a 256 sampled points requires 65536 multiplications with Discrete Fourier Transform calculations, while Fast Fourier Transform only requires 2048 multiplications to obtain the Discrete Fourier Transform.

2.3 Wavelet Transform

The idea of Wavelet transform has been introduced by a French geophysical engineer, Jean Morlet, in 1982. The basic idea of the Wavelet analysis is much similar to the Fourier analysis, where the objective of the both analyses is to expand the functions using a set of basic functions. However, Wavelet analysis perform the expansion in terms of wavelets, which are generated from translations and dilations of a single fixed function called ‘mother wavelet’, in comparison to the use of trigonometric polynomials of Fourier analysis. The idea of ‘mother wavelet’ was first introduced by

Morlet et al. (1982), to achieve good time resolution and high frequency resolution for high frequency transients and low frequency components respectively. The mother wavelet is defined as:

$$\varphi_{a,b}(t) = \frac{1}{\sqrt{|a|}}\ \varphi\left(\frac{t-b}{a}\right), \qquad a, b\ \in R\ , a \neq 0 \tag{19}$$

Where a is called as scaling parameter and the b is called the translation parameter. The scaling parameter evaluates the amount of compression or scale and the translation parameter defines the time location of the wavelet. The wavelets generated using 'mother wavelet' method allows a closer association among the function and their coefficients and it will give a higher mathematical consistency in reconstruction and manipulation (Lee & Yamamoto, 1994).

Although the techniques such as Gabor transform has been developed to analyse the non-stationery signals, wavelets possess a distinctive advantage over those methods in non-stationery signal analysis in signal processing. In Wavelet theory, the mother wavelet generates an orthonormal basis for $L^2(R)$. This is a major advancement in the in the wavelet theory in comparison to Gabor transform (Lee & Yamamoto, 1994).

R denotes the real numbers and the L^2 is the set of all functions f, that have a bounded energy which is defined by:

$$\int_{-\infty}^{\infty} |f(t)|^2\ dt\ <\ \infty \tag{20}$$

2.3.1 Basics of Wavelet Theory

Consider the following conditions for a complex-valued function φ.

$$\int_{-\infty}^{\infty} |\varphi(t)|^2\ dt\ <\ \infty \tag{21}$$

$$\mathrm{C}_{\varphi} = 2\pi \int_{-\infty}^{\infty} \frac{|\hat{\varphi}(\omega)|^2}{|\omega|}\ d\omega\ <\ \infty \tag{22}$$

Where φ is the mother wavelet and the $\hat{\varphi}$ is the Fourier transform of φ. The condition on equation 21, indicates the finite energy of the function and the equation 22 indicates that $\hat{\varphi}(0) = 0$ if the $\hat{\varphi}(\omega)$ is smooth.

2.3.1.1 Continuous Wavelet Transform

If the φ satisfies the conditions of equations 21 and 22, then the Wavelet transform of a function $f(t)$ is defined by the following equation.

$$F(b,a) = \frac{1}{\sqrt{a}} \int_{-\infty}^{\infty} \varphi' \left(\frac{t-b}{a}\right) f(t)dt \tag{23}$$

Where, φ' is the complex conjugate of φ and $b \in R, a > 0$.

Consider the function, $\varphi_{a,b}(t)$, given by equation 19. Then, the equation 23 can be represented as an inner product of the function $f(t)$ as follows:

$$F(b,a) = \int_{-\infty}^{\infty} \varphi'_{a,b}(t) f(t)dt \tag{24}$$

The original signal can be reconstructed by using the inverse Wavelet transform, which integrates the entire projections of the signal on to wavelet basis. The inverse Wavelet Transform is defined as:

$$f(t) = \frac{1}{c_\varphi} \int_{-\infty}^{\infty} \int_{-\infty}^{\infty} F(b,a) \varphi_{a,b}(t) \frac{dadb}{a^2} \tag{25}$$

This behaviour is called the quasi-orthogonality (Sheng, 1996).

The wavelet coefficients obtained by Continuous Wavelet Transform will be highly redundant since, the scaled functions which are used to calculate the wavelet transform are closely related to the orthogonal basis. Moreover, the Wavelet transform has an infinite number of wavelets and the wavelet transform does not possess an analytical solution for most of the functions (Valens, 1999). These properties makes it difficult to use the Wavelet Transform in practical situations. Discrete Wavelet Transform was developed to overcome these drawbacks.

2.3.1.2 Discrete Wavelet Transform

It is vital to use the discrete version of the Continuous Wavelet Transform, since the most of the data in signal processing is in the form of finite number of values. To start with, the scale parameter and the translation parameter has to be discretised.

Let, the scale parameter, $a = a_0^m$ and the translation parameter, $b = nb_0$ in the discrete domain. The discretised wavelets are defined as follows:

$$\varphi_{m,n}(t) = a_0^{-m/2}\varphi\left(\frac{t - nb_0}{a_0^m}\right) \tag{26}$$

Where, $m, n \in Z$. Then, the Discrete Wavelet Transform is defined as:

$$F_{m,n} = \int_{-\infty}^{\infty} \varphi'_{m,n}(t) f(t) dt \tag{27}$$

2.3.2 Different Types of Wavelet Functions

Over the years, few different types of wavelet functions have been developed by various scientists and mathematicians. Haar Wavelet, Meyer Wavelet, Morlet Wavelet and Daubechies Wavelet are some of those different functions with different characteristics. It is important to understand the characteristics of these different wavelet functions to employ the most appropriate function to a unique analysis.

2.3.2.1 Haar Wavelet

The Haar basis is considered as the first orthonormal wavelet basis and it is the simplest version of wavelet function.

Define the function, $\varphi(t) = \emptyset(2t) - \emptyset(2t - 1)$ and presume that the $\emptyset(t)$ satisfies the following:

$$\emptyset(t) = \begin{cases} 1 & if\ 0 \le t \le 1 \\ 0 & otherwise \end{cases} \tag{28}$$

Then, the Haar Wavelet is defined as:

$$\varphi(t) = \begin{cases} 1 & if\ 0 < t \le 1/2 \\ -1 & if\ 1/2 < t \le 1 \\ 0 & Otherwise \end{cases} \tag{29}$$

The function $\emptyset(t)$ is called the Harr scaling function. For its own translations and dilations, the Harr Wavelet, $\varphi(t)$ is orthogonal and the family, $\varphi_{m,n}(t)$ is as follows:

$$\varphi_{m,n}(t) = 2^{-m/2}\varphi(2^{-m}t - n) \qquad m, n \in Z \tag{30}$$

The Haar Wavelet does not possess a good time-frequency localization (Shah, 2015). Figure 2 illustrates an example graph of Haar scaling function and the Haar Wavelet.

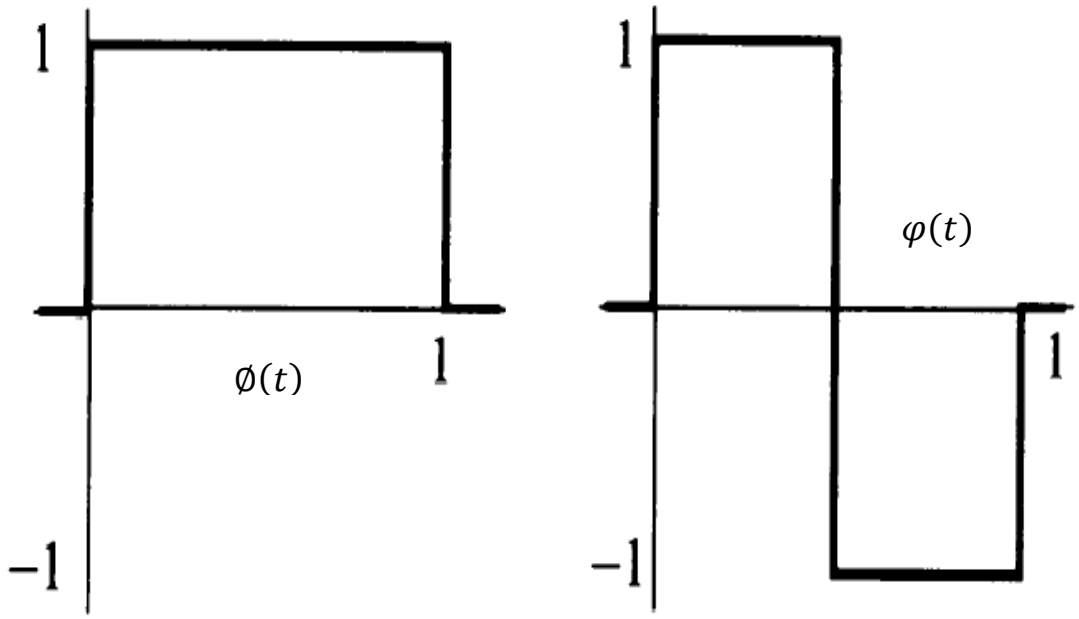

Figure 2: Haar scaling function $\emptyset(t)$ (left) and Harr Wavelet $\varphi(t)$ (right) (Strang, 1993)

2.3.2.2 Daubechies Wavelet

Daubechies Wavelet is a compactly supported orthonormal wavelet, which was introduced by Ingrid Daubechies.

Consider the scaling function $\emptyset(t)$,

$$\emptyset(t) = \sum_{k=-\infty}^{\infty} \alpha_k \sqrt{2}\ \emptyset(2t-k) \tag{31}$$

Where, $\alpha_k \in Z$ and satisfies the following conditions for all integers of $N \geq 2$.

$$\alpha_k = 0 \qquad if\ k < 0\ or\ k > 2N \tag{31}$$

$$\sum_{k=-\infty}^{\infty} \alpha_k\, \alpha_{k+2m} = \delta_{0m} \qquad for\ all\ integers\ m \tag{32}$$

$$\sum_{k=-\infty}^{\infty} \alpha_k = \sqrt{2} \tag{33}$$

$$\sum_{k=-\infty}^{\infty} \beta^k\, k^m = 0 \qquad 0 \leq m \leq N-1 \tag{34}$$

Where, $\beta_k = (-1)^k \alpha_{-k+1}$.

Then, the $\varphi(t)$ is defined as:

$$\varphi(t) = \sum_{k=-\infty}^{\infty} \beta_k \sqrt{2}\, \emptyset(2t-k) \tag{35}$$

The Daubechies scaling function and the Daubechies Wavelet for N = 2, illustrates in Figure 3 and Figure 4 respectively.

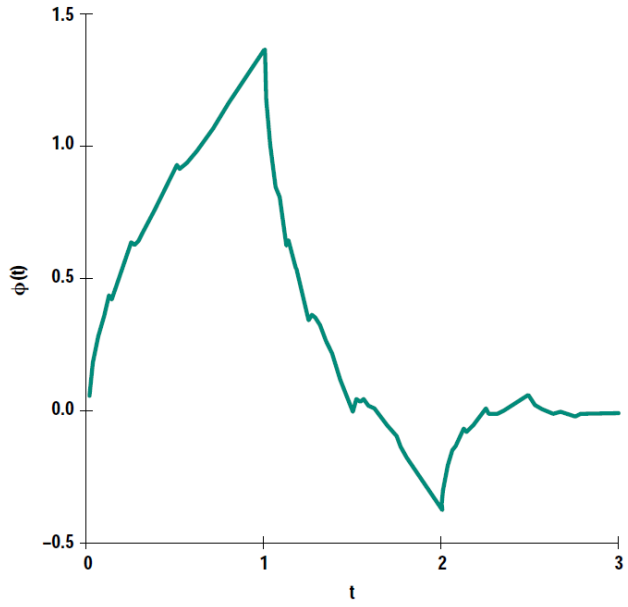

Figure 3: Daubechies Scaling function for N = 2 (Lee & Yamamoto, 1994)

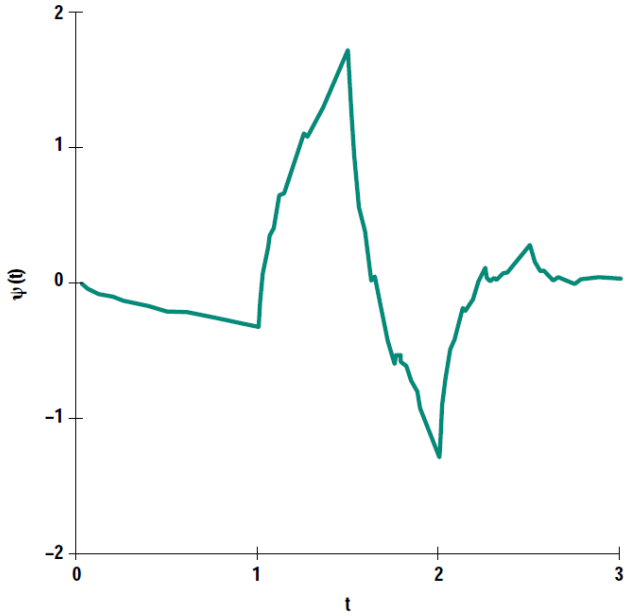

Figure 4: Daubechies Wavelet for N = 2 (Lee & Yamamoto, 1994)

2.3.2.3 Meyer Wavelet

The French mathematician Yves Meyer, introduced a smooth orthonormal wavelet called the Meyer Wavelet. The Meyer Wavelet function, φ can be easily calculated by the Fourier transform of the scaling function.

The Fourier transform $\widehat{\emptyset}(\omega)$ of a scaling function $\emptyset(t)$ is defined as:

$$\widehat{\emptyset}(\omega) = \begin{cases} 1 & if\ |\omega| \leq \frac{2\pi}{3} \\ \cos\left[\frac{\pi}{2}\, v\left(\frac{3}{4\pi}|\omega| - 1\right)\right] & if\ \frac{2}{3}\pi \leq |\omega| \leq \frac{4}{3} \\ 0 & otherwise \end{cases} \tag{36}$$

Where, v satisfies the following conditions:

$$v(t) = \begin{cases} 0 & if\ t \leq 0 \\ 1 & if\ t \geq 1 \end{cases} \tag{37}$$

$$v(t) + v(1-t) = 1 \tag{38}$$

The Fourier transform of φ is given by:

$$\hat{\varphi}(\omega) = e^{i\omega/2}\left[\widehat{\emptyset}\,(\omega + 2\pi) + \widehat{\emptyset}\,(\omega - 2\pi)\right]\widehat{\emptyset}\left({}^{\omega}/_{2}\right) \tag{39}$$

The Meyer Wavelet $\varphi(t)$ can be found by the inverse Fourier Transform. An example of Meyer Wavelet illustrates in Figure 5.

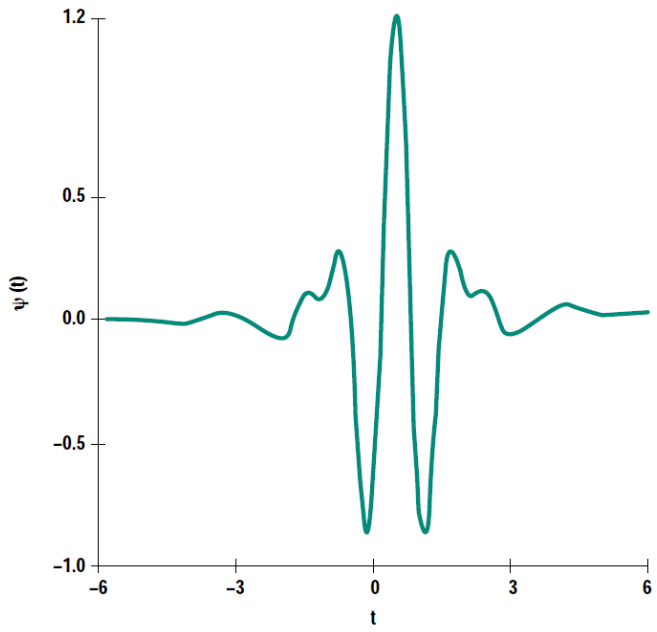

Figure 5: The shape of Meyer Wavelet (Lee & Yamamoto, 1994)

2.3.2.4 Morlet wavelet

Abrupt impulses tend to be occurred in a signal, during a mechanical failure. Since the shape of the Morlet Wavelet is much closer to impulse component (Lin & Qu, 2000), it has been heavily used in fault diagnostics mechanical components. A Morlet Wavelet can be defined as:

$$\varphi(t) = exp\left(\frac{-\beta^2 t^2}{2}\right)\cos \pi t \tag{40}$$

A son wavelet of Morlet Wavelet can be defined as:

$$\varphi_{a,b}(t) = exp\left[\frac{-\beta^2 (t-b)^2}{a^2}\right]\cos\left[\frac{\pi(t-b)}{a}\right] \tag{41}$$

Where, a is the dilation parameter and the b is the translation parameter.

The time resolution and the frequency resolution of the Morlet wavelet depends on the parameter β. When $\beta = 0$ the Morlet wavelet gives the optimum frequency resolution and when $\beta \to \infty$ it gives the optimum time resolution. Thus for a unique signal there is optimal β which gives the finest time – frequency resolution (Lin & Qu, 2000). Figure 6 illustrates the shape of a Morlet Wavelet.

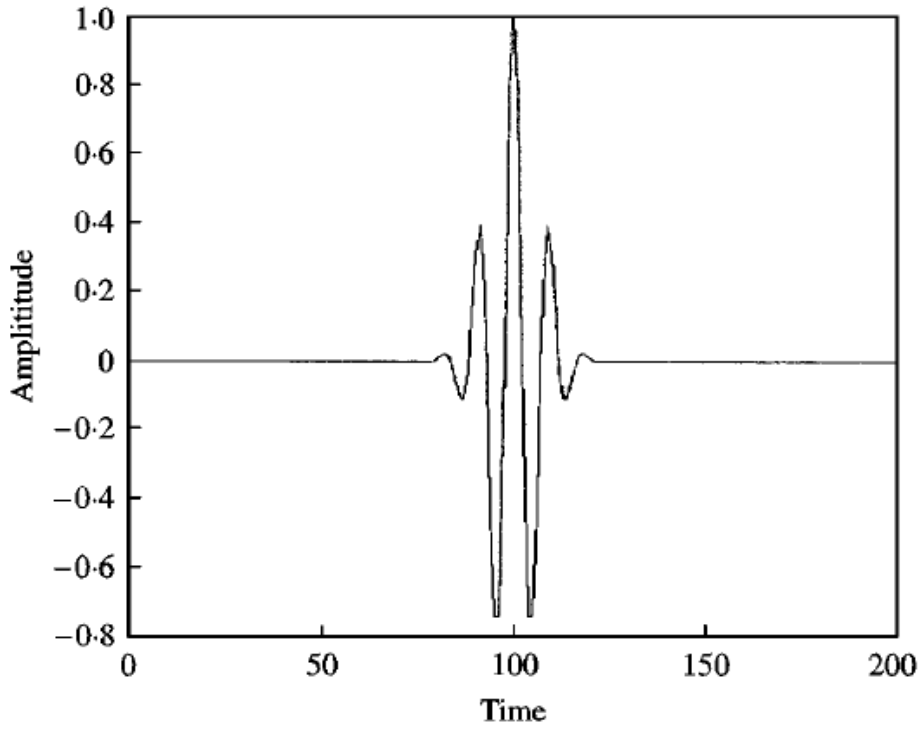

Figure 6: The shape of a Morlet Wavelet (Lin & Qu, 2000)

2.3.3 Multiresolution Analysis (MRA) and Wavelets

The basic idea behind the MRA is to represent a signal with contrasting grades of resolutions, which is achieved by consecutive approximations of the signal. Each of those consecutive approximations gives a smoother version of the signal. Hence, it was called as Multiresolution Analysis.

The idea of MRA is first developed by Mallat and Meyer in 1986 and the findings of S. G. Mallat (1989), introduced an effective numerical algorithm for MRA. The process of describing a signal mathematically in different frequencies is the main component of MRA. It decompose the whole signal space in to different subspaces, thus the each subspace contains a single component of the original signal (Shah, 2015). Thus, the MRA plays a vital role in categorized decomposition of signals into different frequency components.

The subsequent conditions are fulfilled for a series of $V_m(m \in Z)$ closed subspaces which are contained in MRA.

1. $\cdots \subset V_{-2} \subset V_{-1} \subset V_0 \subset V_1 \subset \cdots \subset V_m \subset V_{m+1} \cdots$
2. $\overline{\bigcup_{m=-\infty}^{\infty} V_m} = L^2(R)$,
3. $\bigcap_{m=-\infty}^{\infty} V_m = \{0\}$,
4. $f(x) \in V_m$ if and only if $f(2x) \in V_{m+1}$for all $m \in Z$,
5. $\emptyset_{0,n} = \emptyset(x-n), n \in Z$ where, $\emptyset \in V_0$

   Then, $\|f\|^2 = \int_{-\infty}^{\infty} |f(x)|^2 dx$, for all$f \in V_0$

Where, $\emptyset$ is the scaling function.

It is called that the MRA is generated by $\emptyset$, if

- V_m is a multiresolution of $L^2(R)$ and
- V_0 is the closed subspace produced by the integer translates of the function $\emptyset$.

The scaling function, $\emptyset$, of every MRA is given by:

$$\emptyset(x) = \sum_{n=-\infty}^{\infty} c_n \, \emptyset(2x-n) \tag{42}$$

Then, the Wavelet function is defined as:

$$\varphi(x) = \sum_{n=-\infty}^{\infty} (-1)^n c_n \emptyset(2x - n) \tag{43}$$

The equation 42 is called the dilation equation and it plays a vital role in the final properties of the MRA since, the properties of the basic elements and the wavelet are correlated to each other.

2.4 Summary

Numerous types of waveform analysis techniques are using in tool condition monitoring and fault diagnosis. Fourier Transform and Wavelet Transform are two main signal processing techniques and theories of those techniques have been developed over the years by numerous researchers. Fast Fourier Transform is using as a standard techniques of Fourier Transform to convert the time domain signal in to its frequency components. On the other hand there are different types of Wavelet functions for different purposes which are developed by different researchers including Harr Wavelet, Morlet Wavelet, Daubechies Wavelet and Meyer Wavelet.

CHAPTER 3. SIGNAL PROCESSING TECHNIQUES AS AN AID TO TOOL CONDITION MONITORING (TCM)

It is imperative that the current drilling processes should improve to achieve prime performances, since the development of the lifestyles and overall growth of economy in countries are heavily depend on the modern mining industry. To improve the efficiency in hard rock drilling it is vital to identify the condition of the rock tools. Identifying the rock tool condition in a real time drilling process pose a unique challenge to the drill rig operators because of the dynamic condition of the drilling process. Operators are solely depend on their experience to detect the changes in rock tool condition such as wear of buttons of the drill bits and button failures. This process is not a reliable method and to increase the performances in drilling, a more consistent technique should be introduced.

Over the years researchers have been trying to apply signal processing techniques in tool condition monitoring and fault diagnostics. Fourier Transform and Wavelet Transform are the two main signal processing techniques which have been using to detect the abnormalities in tool conditions. Few types of monitoring techniques (Vibration, Sound, Acoustic emission, etc.) have been using to gather the required data for the signal processing.

The applications of monitoring techniques and signal processing techniques as an aid of tool condition monitoring will be overviewed in this chapter.

3.1 Applications of Monitoring Techniques in Tool Condition Monitoring

It is important to decide on the device wisely according to the required measurement resolution and range to achieve the success in the tool condition monitoring researches. Moreover the sampling frequency of the instrument also plays a major role in successful monitoring, where the norm suggests that the sampling frequency should be large or equal to the twice of maximum frequency. Furthermore, for a given research, the selection of monitoring technique depends on the economic viability of the research outcomes and the feasibility of that monitoring method to detect the tool wear or failure reliably. Vibration, acoustic emission and sound are three major monitoring techniques, which have been using over the years in tool condition monitoring.

3.1.1Vibration

Vibration is a common occurrence with almost every mechanical process, which is defined as the oscillations occur to the opposite directions of an equilibrium point. Over the years, vibration signature of a process has been used to observe the condition of that process and the materials. The vibration signals consists of the adequate quick response time required to detect the variations for on-line monitoring and the signals are robust and reliable (Dimla, 2002). Moreover, it requires lesser amount of instruments to record the vibration signals than the acoustic emission. Thus the vibration signal is considered as one of the most popular monitoring technique in tool condition monitoring and fault diagnostics.

Vibration signal analysis has been used in enormous number of researches to monitor the tool condition. For instance, El-Wardany et al. (1996) introduced a method to detect the failure of small drill bits and to observe the wear of the large drill bits using the vibration signature of drilling. Dimla (2002) researched about the correlation between the tool wear and the vibration signatures and found that, it is viable to identify the different tool wear modes by analysing the vibration signal. The amplitudes of the vibration found to be increased with the advancement of tool wear by Rao et al. (2013) in his research on vibration signal analysis in turning AISI 1040 tube, where a Laser Doppler Vibrometer (LDV) has been used to measure the vibration.

Furthermore, analysing the machine vibration has been extensively used in fault diagnostics. Nagayama et al. (2006) used signal processing techniques to analyse the vibration signals recorded using an accelerometer, to detect the misfiring cylinder of an operational condition heavy machinery multi-cylinder diesel engine. A research has been conducted by Singh and Ahmed (2004) to identify the electrical faults in induction machines using vibration signal analysis.

However, the vibration signal is complex to analyse as it comprise of a mixture of signals generated by few sources of the nearby surrounding. Thus it is challenging to detect the damaged component of a machine, by analysing the vibration signature (Bisu et al., 2012). Difficulty of use and expensiveness of the vibration monitoring sensors and the drawbacks such as complexity of the signal provides an indication to search for more feasible monitoring techniques.

3.1.2 Acoustic Emission

A phenomena of transient elastic waves formed by the rapid discharge of energy from localized sources is known as the Acoustic Emission (AE). The use of AE in tool condition monitoring has been become popular in recent years, because of the reliability of the method and the sensitivity to detect the malfunctions. Relatively superior signal to noise ratio of AE method (Han & Wu, 2013) also provides a great advantage over other conventional monitoring techniques. Thus, this is considered as one of the most precise monitoring techniques in tool condition monitoring.

Iwata and Moriwaki (1977) introduced the use of AE signal to observe the tool wear condition in cutting process and found that the total amount of AE was closely linked to the wear of the tool. The measured AE RMS energy has been used to observe the flank wear by decreasing the sensitivity of the signal to the process constraints during progressive tool wear (Kannatey-Asibu & Dornfeld, 1982). Moreover, AE technique have been used in tool condition monitoring by many researchers, because of the ability to record an uncontaminated AE signal by eliminating the undesirable environmental noise and machine vibrations (Lan & Dornfeld, 1982; X. Li, 2002; Liang & Dornfeld, 1989; Ravindra et al., 1997). The frequency band of the AE signal is much higher than the vibration and the noise, which gives it a distinctive advantage over those monitoring techniques. AE signals show large amplitudes at the time of tool failures such as cracking, chipping and fracture and it can be applied to detect the tool failure during a cutting process (Moriwaki & Okushima, 1980).

In addition to the use of AE for tool condition monitoring, it has also been widely used in grinding process to establish a relationship between sparkout on wheel infeed or out-feed (Dornfeld & Cai, 1984), to show the influence of dressing conditions of the grinding wheels (Inasaki & Okamura, 1985) and to monitor the internal grinding (Inasaki, 1991; Wakuda & Inasaki, 1991). Furthermore, AE has been used for the researches in the field of precision machining to process monitoring of metal optical components (Whittaker & Miller Jr, 1991) and to determine the relationship of AE signals to cutting parameters in diamond turning (Pan & Dornfeld, 1986).

The AE signals has been hardly ever used for rock tool condition monitoring in production mining such as the wear and failures of buttons of drill bits, failure of drill rods or shanks. However, the AE technique has been used to develop a relationship

between the diamond drill bit wear and the AE signal (Karakus & Perez, 2014) and found that the amplitudes of the AE signals tend to decrease with increase of the wear of diamonds. Moreover, an Artificial Intelligence (AI) based AE technology was used to detect the different drilling situations and found that the different drilling situations can be characterised by the variations in AE signals created at the rock - bit interface (X. Sun, 1999).

3.1.3 Sound

The sound emitted by a functioning machine contains lot of information about the operational conditions of that machine (Takata et al., 1986) and there are dissimilarities in sounds emitted in different occasions. For instance, the sound generated at a time of tool failure is different to the sound of a normal machine condition. Thus, the abnormal conditions in a machine condition can be distinguish by analysing the sound generated during the process.

Sound monitoring is a simple and reliable method in tool condition monitoring since, the sound emitted during a process can be collected by a microphone which is located at a neighbourhood vicinity of the machine. A simple microphone is able to detect the high frequency audio signal, which is an inexpensive solution for chatter detection (Cheng, 2008). In addition to that, the sensitivity of the microphone in chatter detection is comparable to other expensive sensors such as accelerometers and plate dynamometers (Kuljanic et al., 2009). However, the sound monitoring method has some limitations as well. The sound signals in the frequency region of 0 Hz to 2 kHz tend to influence by the surrounding noise (Salgado & Alonso, 2007) and the suppression of environmental noise is an important factor to achieve commendable results with the analysis. Furthermore, the sensitivity of the microphone for frequencies below 100 Hz is not adequate (Cheng, 2008) and also the direction of the sensor plays a major role in detecting the required data.

Over the years, the use of sound detection in TCM becomes more popular with the researchers. A dynamic model was developed to understand the relationship between sound emitted during a cutting process and the tool wear, using the sound generated during a machining process by Lu and Kannatey-Asibu (2002). A condenser microphone with a sampling rate of 50 kHz was used to record the sound, by Salgado and Alonso (2007) in their research, to develop a new system for TCM in turning of

AISI 1040 steel. Furthermore, new methodologies were developed with the use of sound detection to monitor the tool wear, by Lu and Wan (2013) in micro-milling of SK2 steel and Samaraj et al. (2011) in a turning process.

In related to the mining industry, laboratory investigations have been conducted to estimate the rock properties by analysing the sound level generated during a hard rock drilling process (Kumar et al., 2011; Vardhan et al., 2009). Gradl et al. (2011) researched the noise characteristics of three different drill bits (Diamond core bit, PDC core bit and Roller cone bit) and concluded that the signature of the noise is clearly related to the design of the drill bit. However, the noise signature produced during a hard rock drilling process still not have been incorporated in to the monitoring of rock tool wear and failures in production mining process.

3.2 Applications of Signal Processing Techniques in Tool Condition Monitoring

Over the years, various types of sensors have been used to collect the data, in aid of tool condition monitoring. As the frantic data collected such as vibration, noise, electric current, comprises of lot of information, which needs to be processed to achieve the required outcomes. One of the most important factors in tool condition monitoring is to select the most appropriate data processing and pattern recognition technique to identify the state of the tool by extracting and enhancing the desired data from a hectic original signal. Few popular signal processing techniques are as follows;

- Time domain analysis
- Frequency domain analysis (Fourier Transform)
- Time – Frequency analysis (Wavelet Transform)

3.2.1 Applications and Drawbacks of Fourier Transform

Fourier transform is regarded as the basis of modern signal processing and it converts a time domain signal into its frequency components (Zhu et al., 2009). Fast Fourier Transform (FFT) have been widely used in various engineering applications, as a standard technique of Fourier Transform, to highlight the distinctive frequencies.

Fourier Transform has been used over the years, to transform the frantic original time domain signal in to an enhanced frequency domain signal to detect the tool condition by numerous researchers. Gradl et al. (2011), used the FFT to accomplish the frequency analysis of the noise data recorded in their research on analysing the noise

characteristics of drill bits. Karakus and Perez (2014), calculated the frequency spectrum using FFT to analyse the effect of diamond core drill bit wear on acoustic emission. Moreover, FFT analysis have been used by S. Li and Li (1990), to find the characteristic frequencies related to the bearing failures, which are utilized in their study on monitoring the bearing condition. Grinding wheel condition monitoring is another popular application, which have been using the frequency analysis (Furutani et al., 2002; Hosokawa et al., 2004; Mokbel & Maksoud, 2000).

However, Fourier transform has some hindrances, which have forced the researchers to seek for new methodologies of signal processing. For instance, it is challenging to observe any abnormal property of the signal ($f(t)$) from the Fourier transform of that signal ($f(\omega)$), as the signal $f(t)$ is integrated for all times to get the Fourier transform (Zhu et al., 2009). Furthermore, The variations of the amplitudes of the vibration measured, which is generated as a result of an unexpected states of the material, tends to generate false alarms with the FFT (El-Wardany et al., 1996). Generally an output signal of a machine process consists of non-stationery components, which are generated due to machine faults and environment changes. Hence, it is crucial to identify those abnormalities in non-stationery components of the output signal. However, FFT techniques are not able to distinguish the characteristic information of the non- stationery signals, hence it is not suitable for the non-stationery signal analyses (Peng & Chu, 2004). Wavelet Transform has been emerged as a more superior signal processing technique to overcome those drawbacks in Fourier Transform.

3.2.2 Wavelet Transform and Its Applications

Wavelet transform is a mathematical process which have been developed for the time - frequency analysis of a signal. It indicates the variation of the intensity of the signal with the changes of time and frequency by transforming the time domain signal in to numerous frequency groups (Nagayama et al., 2006). As a solution for the drawbacks of FFT, Short Time Fourier Transform (STFT) have been introduced and used over the years. However, the time - frequency resolution of STFT is constant because, the same window function is utilized for the calculations at entire frequency range (Singh & Sa'ad Ahmed, 2004). Wavelet Transform has been introduced to overcome the shortcomings of STFT in which the frequency of the signal guides the time – frequency resolution of the Wavelet Transform. The wavelet attains a high time resolution at

higher frequencies whereas, the time resolution is low at lower frequencies. The frequency resolution and time resolution is completely different at higher frequencies, where it reaches a low frequency resolution and high time resolution (Peng & Chu, 2004).

The variation of the frequency component with the time, of a non – stationery signal can be clearly illustrated by a wavelet scalogram. The analysis of wavelet phase map is challenging in comparison to the scalogram. However, it is useful in identifying the signal discontinuities and impulses. With the wavelet phase spectrum, a taper will be precisely connected with the every signal discontinuity, regardless of the wavelet function used. Some researchers have compared wavelet transform with other analysis methods for tool condition monitoring. The Wavelet analysis is less time consuming in comparison to the Envelope Detection (ED) method for fault diagnosis of rolling element bearing, although the both methods are effective in detecting the faults (Peter et al., 2001). The experiments conducted to compare the effectiveness of Wavelet transform, FFT and Hartley transform concludes that the Wavelet transform provides superior results than other methods in tool condition monitoring feature extraction for DC power system and solar power distribution system (Momoh & Dias, 1996; Momoh et al., 1995). The sensitivity and robustness of Wavelet transform is compared with the phase and amplitude demodulation and beta kurtosis methods in gear damage monitoring and the results concluded that the wavelet transform technique gives much superior results over the other methods (W. Q. Wang et al., 2001).

With the increased popularity of Wavelet transform, Newland published few papers which describes the theory of the technique and the applications of the method in vibration analysis (D. Newland, 1995; D. E. Newland, 1994). Over the years, Wavelet transform has been successfully used in several applications in tool condition monitoring and machine fault diagnosis. Few of the main applications are as follows;

- Time – frequency analysis
- Fault feature extraction
- Singularity detection
- Wavelet denoising

3.2.1.1 Time – Frequency Analysis of Signals with Wavelet Transform

Time – Frequency analysis with Wavelet transform uses numerous measures of the transformed signal in aid of tool condition monitoring which includes, scalogram, scaling coefficient, statistics of wavelet matrix and wavelet coefficients. Time – frequency analysis with wavelet transform has been used in wide range of applications. Analysis of gear vibration signals in condition monitoring and fault diagnosis was one of the most prominent uses of Wavelet transform during the introduction period of the technique. Wang and McFadden applied Wavelet transform to analyse the gearbox vibration in few researches including gearbox vibration analysis (W. Wang & McFadden, 1993), early gear damage detection (W. Wang & McFadden, 1995) and fault detection by analysing the gearbox vibration (W. Wang & McFadden, 1995). The results demonstrated that the simultaneous detection of various types of incipient mechanical failures of gears is viable, with the analysis of vibration signal through Wavelet transform. Numerous other researchers have also used Wavelet transform technique in fault detection in gear systems (Brennan et al., 1997; Sung et al., 2000; Yesilyurt & Ball, 1997). Furthermore, the Wavelet transform has been widely used in crack detection of rotor systems and the structures by several researchers (Adewusi & Al-Bedoor, 2001; Quek et al., 2001; Zhang et al., 2002; Zou et al., 2002). Wavelet transform technique has been used to identify the diesel engine malfunctions. Nagayama et al. (2006), conducted a research to detect the misfiring cylinder of a working condition multi – cylinder heavy machinery diesel engine using Wavelet analysis.

Another important application of Wavelet transform is the identification of drill bit wear and breakage. For instance, X. Li et al. (1999) introduced a method for tool breakage monitoring using Discrete Wavelet transform of acoustic emission and Gong et al. (1997) used Wavelet analysis to monitor the tool wear condition in turning. Besides those, numerous researchers have been used Wavelet transform in aid of drill bit condition monitoring (Fu et al., 1996; Mori et al., 1999).

As explained before, the time – frequency analysis with wavelet transform has a distinctive advantage over the other signal processing methods. However, this technique also has some drawbacks. One of the main disadvantages of Continuous Wavelet transform in time – frequency analysis is overlapping, which can be occurred due to a large number of redundant data. The overlapping may obstruct the exact

condition of the scalogram and it will misinterpret the signal analysis. Peter et al. (2004), introduced a novel method called Exact Wavelet analysis to minimize the effects of overlapping. Moreover, the signals which are polluted with the noise cannot be precisely analysed, since the phase spectrum of the wavelet transform is highly sensitive to the background noise. Besides those problems, the coefficients generated by conventional continuous wavelet transform methods may be different at different scales, which may produce diluted and distorted features in the results (Peter et al., 2004).

3.2.2.2 Singularity Detection with Wavelet Transform

In signal processing, singularity is considered as a sudden change of signal's value to a different amount, which may occurred due to a tool breakage of chipping of material. Weak singularity points of a signal can be disguised by the polynomial trends of that signal. In comparison to some other signal processing techniques, Wavelet transform can eliminate those polynomial trends to distinguish the weak singularity points (Peng & Chu, 2004). The robustness and the effectiveness of highlighting the weak singularity points gives a distinctive advantage for the Wavelet based techniques.

The theory of singularity detection with Wavelet transform has been presented by S. Mallat and Hwang (1992). Numerous researchers have used singularity detection with wavelet transform various applications in tool condition monitoring. For instance, Chen and Li (2006), introduced a singularity detection method with wavelet resolution coefficient norm to analyse the tool condition. Furthermore, the usage of Wavelet transform in singularity detection is widespread into different applications including, bearing fault diagnosis (Q. Sun & Tang, 2002), power system fault analysis (Qing-Quan et al., 2001; Xinzhou et al., 1997), and many more.

Despite the Wavelet transform technique is more effective in singularity detection, the regularity should be considered, when choosing the wavelet function to address a unique issue. Whenever the selected wavelet is not adequately consistent, some of the singularities of the signal might be overlooked. Moreover, it is vital to conduct the pre-processing of the signal to eliminate the noise, to confirm that the influence of the noise for the performances of wavelet is minimised (Chen & Li, 2006).

3.2.2.3 Usage of Wavelet Transform in Feature Extraction

Feature extraction in tool condition monitoring is another extensively used application in Wavelet transform. It is vital to extract the wavelet coefficients to characterize the various tool states in tool condition monitoring. The Wavelet transform has the ability to exhibit the signal with finite number of coefficients since, most of the coefficients are very small and elimination of those will not generate a significant error to the signal (Peng & Chu, 2004). Hence, these coefficients can be extracted and use as fault features in tool condition monitoring, where the feature extraction approaches are commonly established on statistical measurements such as mean and variance to maximise the ability to distinguish between different tool conditions.

Feature extraction with Wavelet transform has been widely used by various researchers in tool condition monitoring. The root mean square (RMS) value of the coefficients has extracted as the fault features by Choi et al. (2004), in their study of the trends of cutting forces with the variation of the tool wear in ramp cut machining. Wu and Du (1996), used Wavelet packet transform technique and proposed an automatic feature extraction and computation method. Tansel et al. (1993), used this technique to predict the micro drill bit breakage in peck drilling by utilizing discrete wavelet transform coefficients of the thrust force.

Furthermore, the usage of feature extraction with Wavelet transform has been extended in to different applications including machine condition diagnosis, structural damage detection. Liu et al. (1997), studied the faults of ball bearings in machines with wavelet packet coefficients and results demonstrated that the higher sensitivity of the coefficients to the faults makes it easier to detect those faults. A new methodology for machinery fault diagnosis using wavelet feature extraction was introduced by Liu and Ling (1999), and concluded that the proposed methodology displays better performance in detecting diesel engine malfunctions. The wavelet feature extraction has been used for the structural damage detection by (C.-J. Lu and Hsu (2000)). The results indicated that maximum variation of the coefficients are generally related to the location of the damage since, minor localised damages were heavily connected with the variations of the wavelet coefficient.

Although the Wavelet transform has been used in wide range of applications including time – frequency analysis, feature extraction and singularity detection, the

unavailability of a standard technique to select the most suitable wavelet function for a unique task is diminishing the popularity of the use. Furthermore, the results derived by different wavelet functions for a unique problem may be different, which will mislead the users of the wavelet transform. The answers for these drawbacks will increase the usage of wavelet transform technique in the future.

3.3 Summary

Numerous types of monitoring techniques are in use for tool condition monitoring and fault diagnostics including, vibration, acoustic emission and sound. Fourier Transform and Wavelet Transform has been widely used in analysing the signals in tool condition monitoring. Time frequency analysis, singularity detection and feature extraction are some of the uses of Wavelet Transform in signal processing.

The most suitable methodology for this research have selected after a comprehensive analysis of the literature on monitoring techniques and signal processing techniques.

CHAPTER 4. APPARATUS SETUP AND TESTING PROCEDURE

4.1 Field Test Site

The mine site, where the experiments were conducted is located in Queensland, Australia. Underground operations have been conducted to extract a copper orebody, using sub level stoping method. The mine area is composed of brecciated granitic rock masses which contains several orebodies with complex veins of chalcopyrite.

The experiments were conducted in an underground stope that contains hard abrasive rock, which is approximately 1.7 km deep from the surface. The drilling surface used for the experiment is shown in Figure 7.

Figure 7: Drilling Surface

4.2 Apparatus setup

The drilling was done by a Sandvik AXERA 7 twin boom jumbo drill rig. A GoPro camera was mounted on top of the windscreen of the drill rig, where the distance between the camera and the drilling face is about 10m. Since the experiment was conducted in an underground stope, the sound is going to reflect along the walls. Thus, the sound generated as a result of drilling process also can be detected with the in-built microphone of GoPro Camera, as same as the other sounds including the engine of the drill rig. GoPro camera captured the video of 170 degrees field of view with 1280 × 720 pixels at a rate of 60 frames per second. The sound of drilling was recorded with the use of the built-in mono microphone of the GoPro camera. It has recorded the sound using 128kbps Advanced Audio Coding (AAC) compression at 48 kHz

sampling rate. The recorded data was transferred in to a personal computer for the analysis. Figure 8 shows the schematic view of the experimental setup.

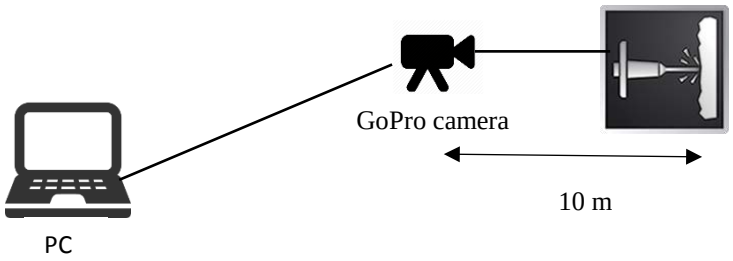

Figure 8: Schematic view of the experimental setup

4.3 Experimental Procedure

Sandvik AXERA 7 twin boom jumbo drill rig was used to drill four meter holes in to a Brecciated granite waste rock. Holes were drilled simultaneously by using Poly Crystalline Diamond (PCD) tapered button bit of 45mm diameter. A picture of both booms drilling simultaneously is shown in Figure 9.

Figure 9: Two booms drilling simultaneously

The drill rig applied a 160 bar percussion pressure, 80 bar feed pressure and 55 bar rotation pressure with 220rpm rotation speed to achieve a penetration rate of 31 mm/s approximately. Video and sound was recorded while drilling using the GoPro Camera, which was mounted on the top of the windscreen of the drill rig. Table 1 shows the drilling specifications of the experiment.

Table 1: Drilling Specifications

Parameters	Description/Measurement
Type of Drill Rig	Sandvik AXERA 7 twin boom Jumbo drill rig
Type of bit	PCD tapered button bit
Rock type	Brecciated granite
Diameter of bit	45mm
Percussion pressure	160 bar
Feed pressure	80 bar
Rotation pressure	55 bar
Water pressure	18 bar
Rotation speed	220 rpm
Penetration rate	31 mm/s

Drill bits of both booms were inspected after 1287.0 s from the start of drilling and identified that one gauge button of the right boom bit was broken. Drilling was started again after the inspection and continued until the whole face was drilled. Upon inspection of bits at the end of the drilling process another gauge button of the right boom bit was identified to be broken. Inspecting of bits after 1287.0 s is shown in Figure 10 and the pictures of the bits before and after the gauge button failure is shown in Figure 11.

Figure 10: Inspecting the bits after 1287.0 s

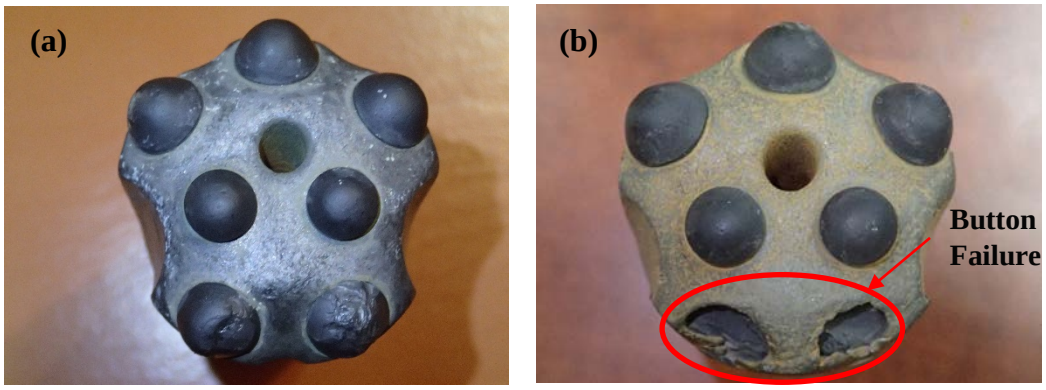

Figure 11: Pictures of the bit (a) Before failure (b) After failure

The sound was extracted from the recorded video data and sound data (WAV format) was separated in to 10 seconds periods. Then the video data was carefully analysed for those time periods to check the status of the drill rig which are,

1. Drilling with only right boom
2. Drilling with only left boom
3. Drilling with both booms simultaneously
4. Not drilling

Sample data sheet of drilling status of the drill rig is shown in *Table 2*.

The sound data was converted to Comma Separated Values (CSV) format for further analysis. After converting to the CSV format, the data sheet consist with 48000 data per one second.

Table 3 illustrates a sample CSV data sheet of the converted sound data. The data sheets for above mentioned time periods were imported in to OriginPro software and Geo-Lab Analyser software to analyse the data with waveform analysis techniques such as Fourier Transform and Wavelet Transform.

Table 2: Sample data sheet of the status of the drill rig

Video	Time (s)		Remarks (Drilling)			
			Left boom	Right Boom	Both	Not Drilling
G62	0	10				
	10	20				
	20	30				
	30	40				
	40	50				
	50	60				
	60	70				
	70	80				
	80	90				
	90	100	**92s**			
	100	110				
	110	120				
	120	130			**120s**	
	130	140				
	140	150				
	150	160				
	160	170				
	170	180				
	180	190				
	190	200		**197s**		
	200	210				
	210	220				

: Left boom only **: Both booms drilling**

: Right boom only **: No drilling**

Table 3: Sample CSV datasheet of a converted sound data

Time (s)	Amplitude (p.d.u)
300	2129
300.00002083	4080
300.0000417	6641
300.0000625	7069
300.0000833	3142
300.0001042	-3930
300.00012498	-9831
300.0001458	-12114
300.0001666	-12324
300.0001875	-11921
300.0002083	-10884
300.00022913	-10127
300.00025	-10030
300.0002708	-8816
300.0002916	-5385
300.0003125	137
300.00033328	7579
300.0003541	14387
300.0003749	17070
300.0003958	17003
300.0004166	17611
300.00043743	17520
300.0004583	13853
300.0004791	7799
300.0004999	1916
300.0005208	-2903
300.00054158	-6454
300.0005624	-8588
300.0005832	-8065

4.4 Summary

The experiment was conducted in an underground mine in Queensland, Australia in collaboration with Mitsubishi Materials Corporation. The video and the sound was recorded during real time drilling process which used a 45 mm diameter PCD tapered button bit. The drill bits were inspected after 1287.0 s and found that one gauge button of the right boom drill bit was broken. The sound data was analysed with waveform analysis techniques using OriginPro and Geo-Lab Analyser software to find the exact moment of button failure.

CHAPTER 5. EXPLORATORY DATA ANALYSIS PROCEDURE

Data analysis is a critical part in the research, which has to be done systematically. The analysis procedure has been divided in to two main categories.

- Video data analysis.
- Sound data analysis to find the button failure.

OriginPro and Geo-Lab analyser are the two main software used to analyse the CSV data file of the sound data. Time series graphs, Fast Fourier Transform (FFT) graphs and Wavelet Transform graphs were created using those software to find the results of the research. The time period of 600 s to 900s after the start of drilling will be used as an example to present the detailed analysis procedure and it is identical for all the other time periods.

5.1 Video Data Analysis

Recorded video of the real time drilling process in an underground mine site is the main data in this research. Video data was analysed to find the status of the drill rig. The video was checked carefully and differentiated the drilling condition in to following four categories.

- Drilling with only right boom.
- Drilling with only left boom.
- Both booms are drilling simultaneously
- Not drilling

The starting time and the end time of the above scenarios are documented in a Microsoft Excel data sheet. Table 4 illustrates the example Excel data sheet for 600s to 900s. According to the data sheet shown in Table 4, only left boom is drilling until 605s where right boom started drilling at that time. Both booms were drilled simultaneously until 621s, where left boom stopped and changed to a different point on drilling surface to start the drilling of hole number 4. It started the drilling again at 643s and both booms were operated concurrently until the right boom finished the drilling of hole number 4 at 746s. Only the left boom was operated from 746s to 781s. Right boom started drilling again at 781s, while the left boom finished the drilling of

hole number 4 at 813s. Right boom operated by itself for 24s until the left boom started the drilling of hole number 5 at 837s.

Table 4: Data sheet of the status of the drill rig (600s-900s)

Video	Time (s)		Remarks (Drilling)			
			Left boom	Right Boom	Both	Not drilling
G64	600	610			**605s**	
	610	620				
	620	630		**621s**		
	630	640				
	640	650			**643s**	
	650	660				
	660	670				
	670	680				
	680	690				
	690	700				
	700	710				
	710	720				
	720	730				
	730	740				
	740	750	**746s**			
	750	760				
	760	770				
	770	780				
	780	790			**781s**	
	790	800				
	800	810				
	810	820		**813s**		
	820	830				
	830	840			**837s**	
	840	850				
	850	860				
	860	870				
	870	880				
	880	890				
	890	900				

: Left boom only
: Right boom only
: Both booms drilling
: No drilling

5.2 Sound data Analysis to find the button failure

The sound recorded by the simple in-built microphone of the GoPro camera was extracted from the video using the EcoDeco TooL software, which creates a WAV file. Then the WAV file was converted to the Comma Separated Values (CSV) format to import the data into the analysis software, which are OriginPro and Geo-Lab analyser.

CSV files of the time periods where only right boom is working and both booms working simultaneously were analysed, since we already know that the button failure occurred in the right boom button bit. The results from the video data analysis was used to differentiate the required time periods. Following signal analysis techniques were used to find the button failure by using the CSV data files.

- Time Series Analysis
- Fast Fourier Transform (FFT) Analysis
- Wavelet Transform Analysis

5.2.1 Time Series Analysis

Time series analysis was conducted using the OriginPro software to find any abnormalities in the sound wave at the time of button failure. Sample image of the interface of the OriginPro software is illustrated in Figure 12. Time series graphs were created and they were analysed visually and statistically.

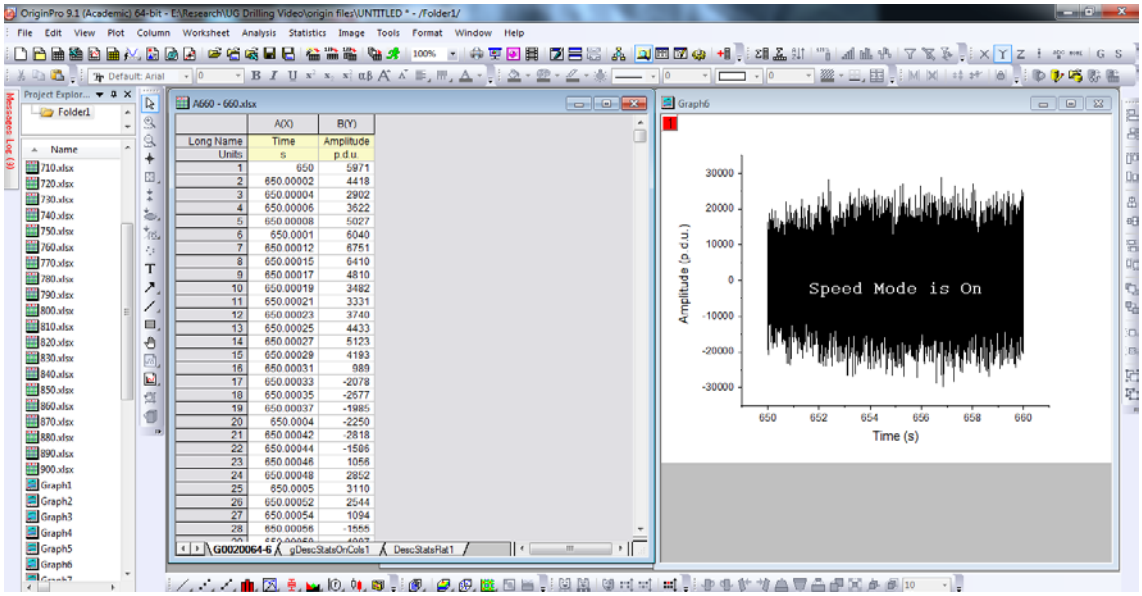

Figure 12: Sample Image of the interface of the OriginPro software

5.2.1.1 Visual analysis of time series graphs

Time series graphs were created for each 10s time periods from the start of the drilling until the time of inspection of the drill bit. The graphs are divided in to the categories according to the status of the drill rig, which are only right boom is working, only left boom is working and both booms are working simultaneously. Figure 13 and Figure 14 shows the time series graphs and their expanded views, where only right boom is working and both booms are working respectively.

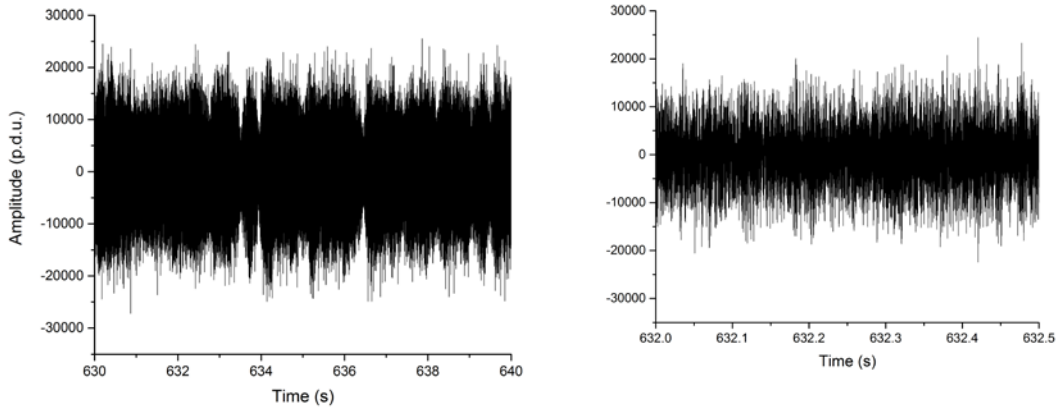

Figure 13: Time series graph - Only right boom is working (L) – Normal view 630s - 640s (R) Expanded View 632s – 632.5s

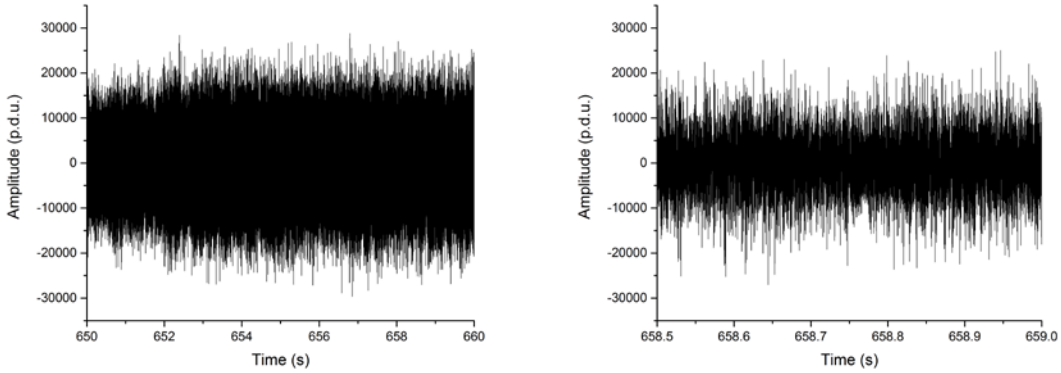

Figure 14: Time series graph - Both booms are working simultaneously (L) Normal view 650s - 660s (R) Expanded view 658.5s - 659s

All the time series graphs were visually analysed from the start to 1287s. As there are 48000 data per one second, the time series graph is too complex to analyse visually. Thus the statistical analysis was conducted.

5.2.1.2 Statistical analysis of Time series graphs

Minimum, maximum and average amplitudes were calculated for the 10s time periods from start of drilling until the inspection of button bit. The minimum, maximum and average amplitude values for the time periods of both booms are working simultaneously were separated and analysed to find any abnormalities at the time of bit button failure. Figure 15 illustrates the changes in the minimum and maximum amplitudes of the sound wave during 600s to 900s time period and Figure 16 shows the variation of average amplitude of the sound wave over the same time period, while both booms are working simultaneously.

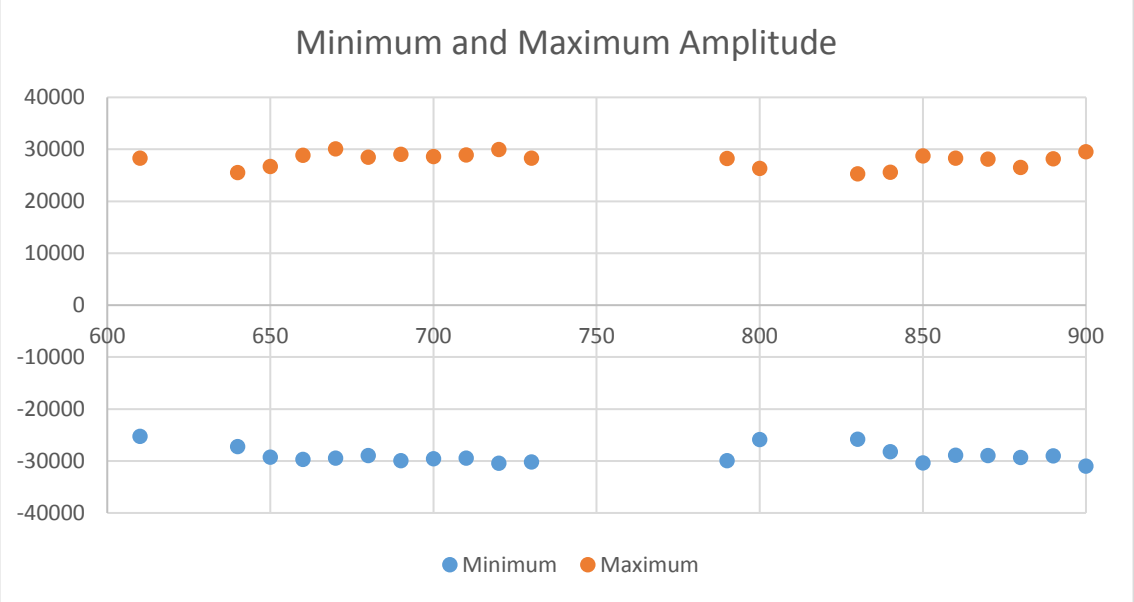

Figure 15: Minimum and Maximum amplitude – Both booms working simultaneously (600s-900s)

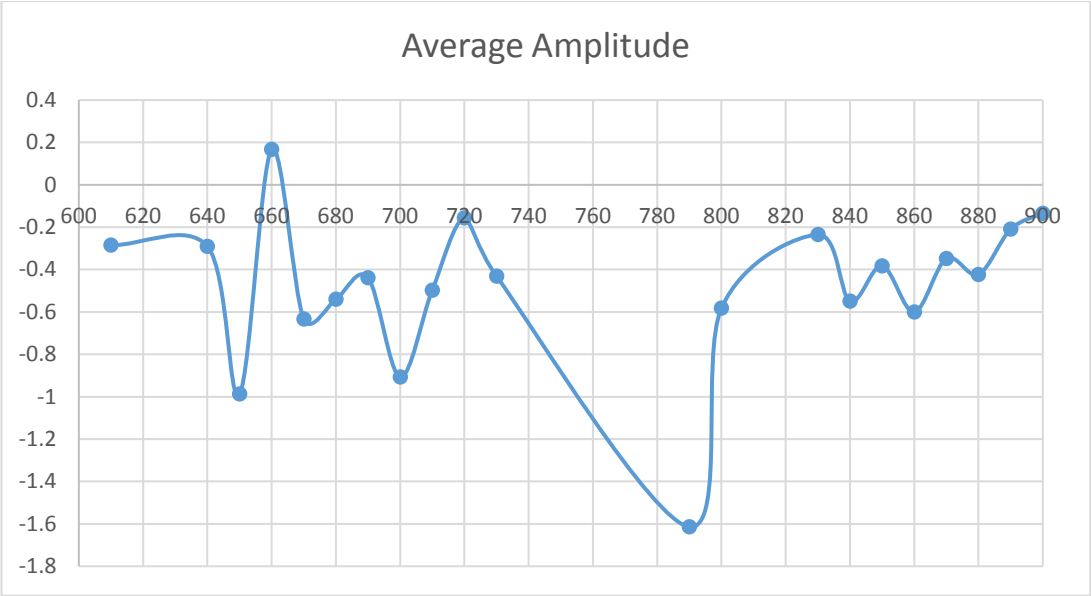

Figure 16: Average amplitude – both booms working simultaneously (600s-900s)

5.2.2 Fourier Transform Analysis

Fourier transform is used to convert the time domain signal in to a frequency domain signal. As a standard technique of Fourier Transform, Fast Fourier Transform (FFT) is used to convert the data in to the frequency domain. The calculations were done using the OriginPro software and it automatically creates the frequency graphs. Prior to the analysis, the frequency graphs were classified according to the status of the drill rig in to the three main categories mentioned above. Then the frequency graphs were analyse visually and statistically for the circumstances, where both booms working simultaneously and only right boom is working.

5.2.2.1 Visual analysis of Frequency graphs

The frequency graphs for the above two circumstances were carefully observed from the start of drilling until the inspection of the drill bit. The procedure was carried out to find any differences in amplitudes of the frequency graphs, before and after the button failure to discover the time of the failure. Frequency graph of a 10s time period, where only the right boom is working illustrates in Figure 17. Figure 18 shows the frequency graph of a 10s time period, where both booms are working simultaneously.

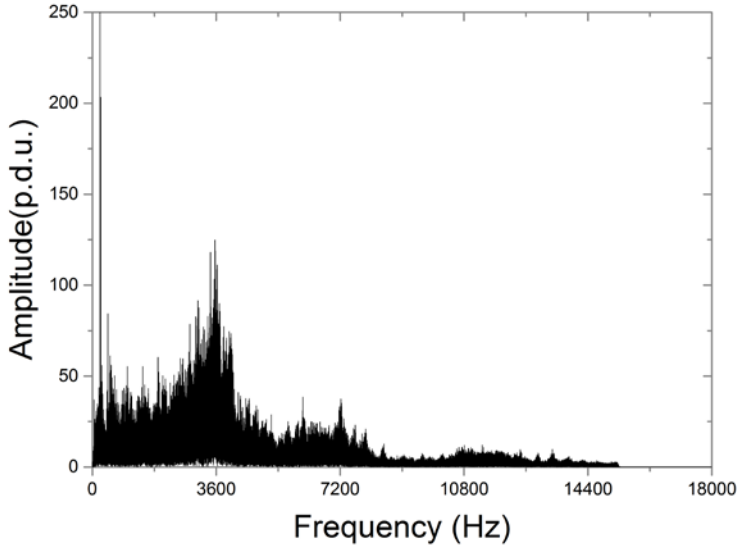

Figure 17: FFT graph - Only right boom is working (630s - 640s)

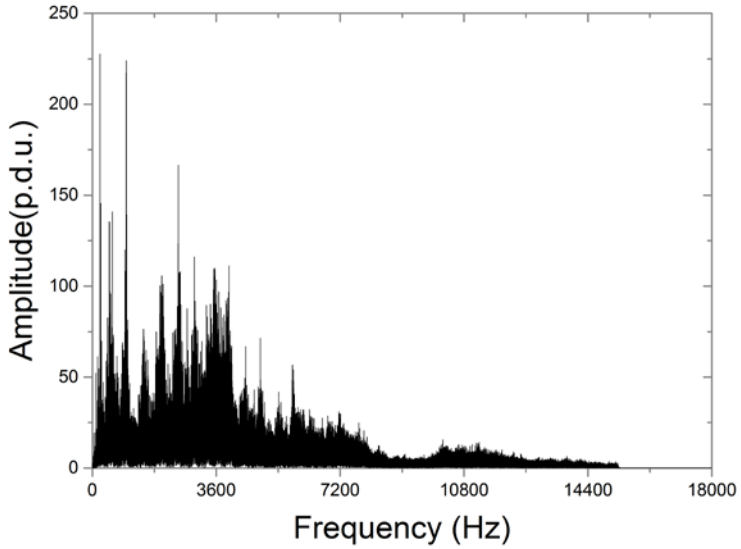

Figure 18: FFT graph - Both booms are working simultaneously (650s - 660s)

During the drilling operation sound emits within a large range of frequency spectrum that is from 0 Hz to 15 kHz, which makes it difficult to analyse. Thus the graphs were carefully examined and separated the frequency range of 4.2 kHz to 8.2 kHz as the dominant frequency range for the statistical analysis.

5.2.2.2 Statistical analysis of Frequency Graphs

The frequency range of 4.2 kHz to 8.2 kHz was divided in to 500 Hz subdivisions for further analysis. For all those divided frequency ranges integrated amplitude was

calculated for the 10s time periods from the start of drilling until the time of inspection of the drill bit. Figure 16 illustrates a sample image of the analysed frequency range for the time period of 690s to 700s.

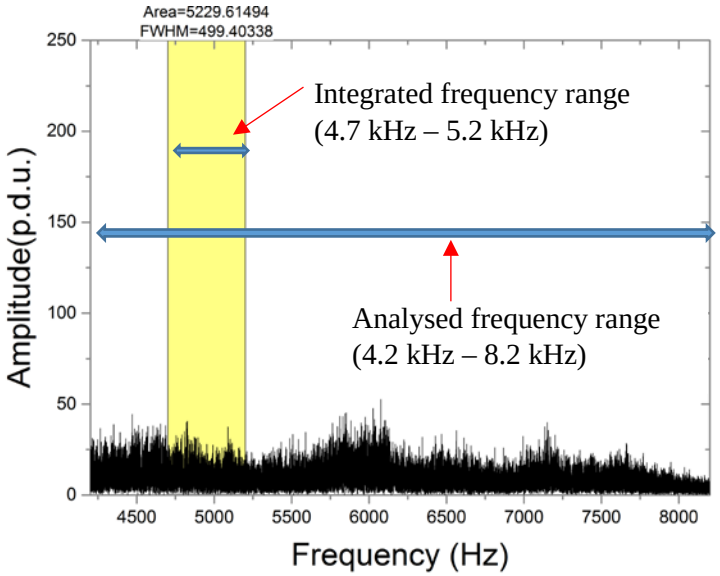

Figure 19: Sample image of the analysed frequency range (4.2 kHz - 8.2 kHz)

The graphs were created between the time and the integrated amplitude for each frequency group to identify the abnormalities and to further narrow the button failure affected frequency range and time frame of which the button failure occurred. Figure 20 and Figure 21 illustrates the variations in integrated amplitudes in frequency ranges of 4.2 kHz to 4.7 kHz and 5.7 kHz to 6.2 kHz respectively in the conditions of both booms are working simultaneously.

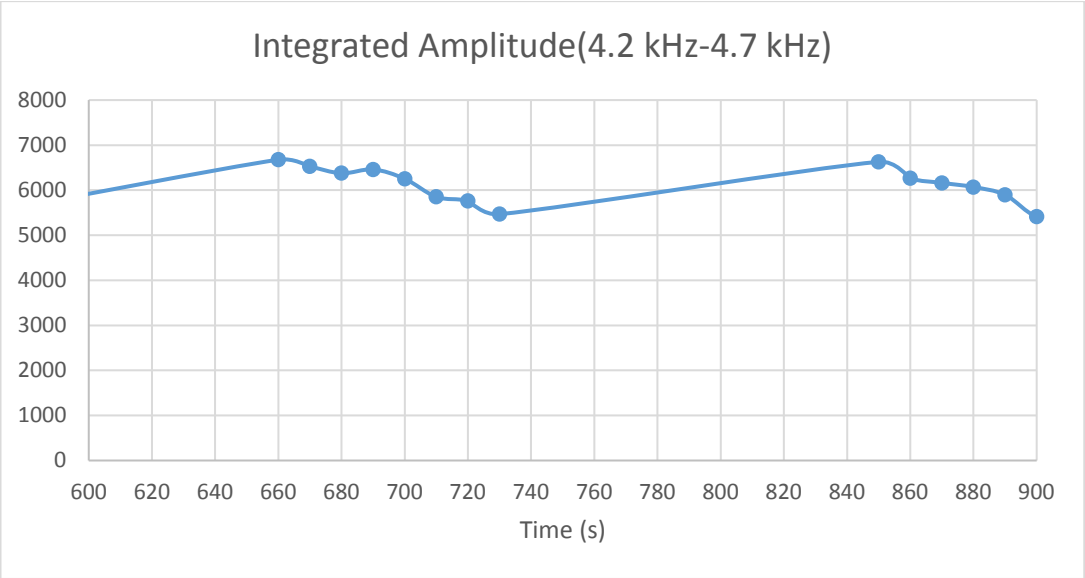

Figure 20: Variation of integrated amplitude (4.2 kHz - 4.7 kHz) - Both booms are working simultaneously

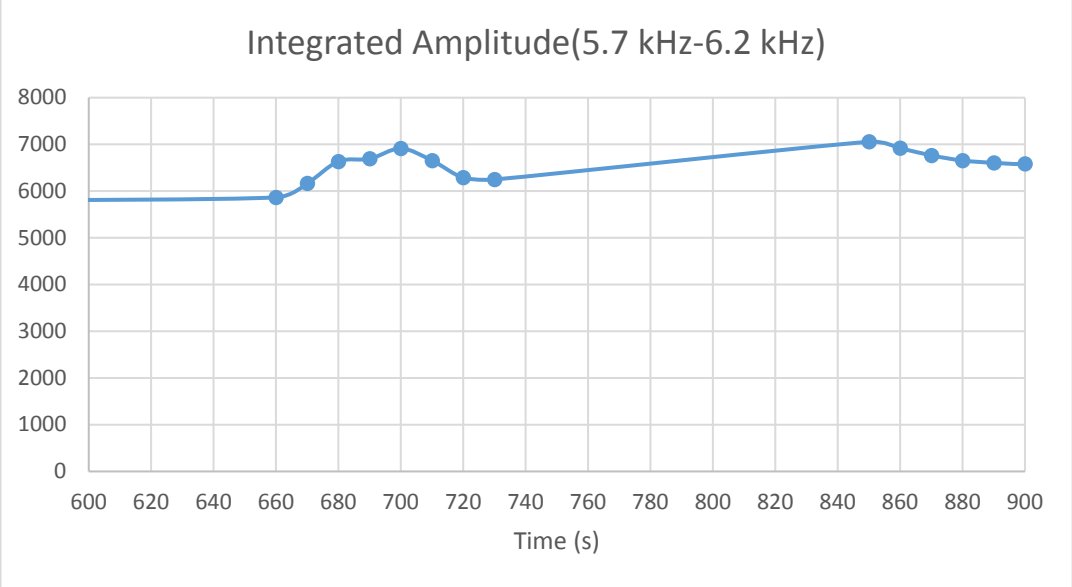

Figure 21: Variation of integrated amplitude (5.7 kHz - 6.2 kHz) - Both booms are working simultaneously

The graphs were analysed and the time frame which the button failure occurred was narrowed down to 30 seconds and also found the button failure impacted frequency range. The wavelet transform analysis was conducted only for that 30 seconds time period.

CHAPTER 5: Exploratory Data Analysis Procedure

5.2.3 Wavelet Transform Analysis

Wavelet transform converts the time domain signal in to different frequency groups and shows the fluctuations of the intensity of the wave with the changes of time and frequency. The selected 30 seconds time period, where the both booms are working simultaneously, was further divided in to 0.2s small time periods for calculation purposes. The wavelet matrix was created using Geo-Lab Analyser software for every 0.2s time periods. Time - Frequency graphs were generated by importing the wavelet matrix in to the OriginPro software. Then the time – frequency graphs were visually analysed to find the high intensity points, which can be occurred at a time of button failure.

5.2.3.1 Visual analysis of Time – Frequency spectrum

All the graphs generated were carefully examined and compared to each other to distinguish the high intensity point, which is related to the button failure of the right boom drill bit. By analysing the graphs, the exact moment of the button failure and the frequency range which is related to the button failure was found. As an example Time – Frequency spectrum for the time period of 650.0s to 650.2s illustrates in Figure 22.

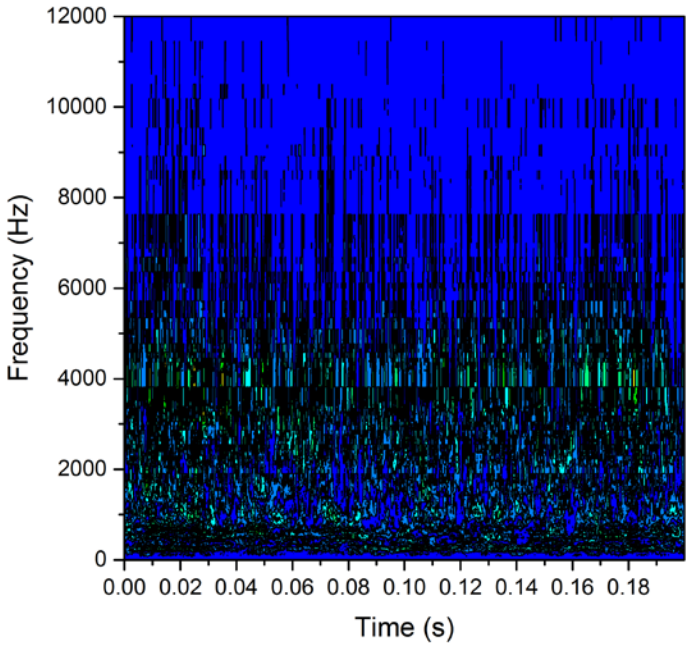

Figure 22: Time - Frequency spectrum (650.0s - 650.2s)

After the discovery of the button failure through visual analysis, statistical analysis was carried out to correlate the average intensity and the maximum intensity, before and after the button failure.

5.2.3.2 Statistical analysis of Time – Frequency Spectrum

Two time arrays were created for the analysis purposes.

1. Between two predefined time periods before the breakage (491.0s – 499.0s)
2. From the breakage point to a different predefined point (650.0s -658.6s)

For those two time arrays maximum intensity was determined by analysing the wavelet matrix between 500 Hz to 600 Hz frequency range, as the singularity point occurred during the button failure is within this frequency range. Average intensity was calculated for the same time arrays between 5.7 kHz to 6.2 kHz using the same wavelet matrix, as there is a slight escalation in integrated amplitude in this frequency range after the button failure. For all the values 9 point moving average was calculated to smooth out the data and to understand the trends. Figure 23 shows the variation of maximum intensity and average intensity before the button failure (491s – 499.2s).

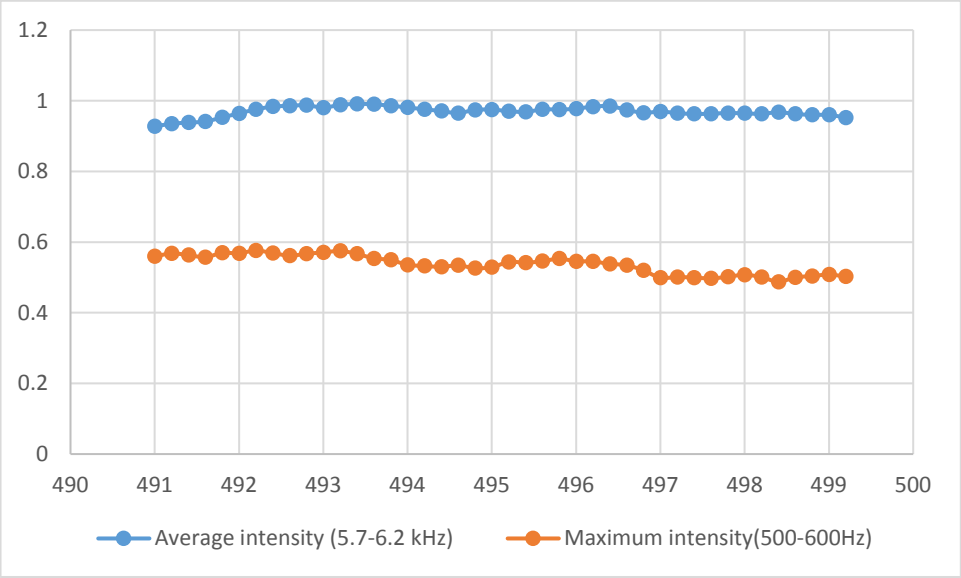

Figure 23: Variation in Average intensity (5.7 kHz - 6.2 kHz) and Maximum intensity (500 Hz -600 Hz) - 491s to 499.2s

Then the combined graph of before and after the button failure was generated to correlate the button failure with the changes of intensity.

5.2.4 Analysis of penetration rates

After a button failure of a drill bit, the penetration rates tends to decrease. Thus real time drilling rates were analysed to correlate the penetration rate and the button failure. The video data was analysed to determine the time conceded to drill each and every hole. The recorded times were divided in to two categories which are holes drilled by right boom and holes drilled by left boom. Table 5 illustrates the time conceded to drill each and every four meter hole. Then the penetration rates were analysed before the button failure and after the button failure to further support the claim of the exact time of button failure through wavelet transform.

Table 5: Time conceded to drill a four meter hole

Hole No	Time(s) /hole (Right boom)	Time(s)/hole (left boom)
1	139	105
2	125	113
3	133	151
4	141	170
5	143	131
6	160	136
7	170	109
8	200	116
9	178	103
10	168	134
11	188	109
12	196	125
13	189	110
14	163	112
15	162	134
16	161	133
17	203	138
18	0	148
19	0	132
20	0	127

5.3 Summary

Video data was analysed to differentiate the status of the drill rig at different time periods. Waveform analysis techniques including time series analysis, Fourier Transform and Wavelet Transform are used to find the exact moment of button failure of the drill bit by analysing the sound recorded during the drilling process. The penetration rate, was calculated by analysing the video data and the results were correlated to the findings of the waveform analysis techniques.

CHAPTER 6. TEST RESULTS AND DISCUSSION

In this chapter the results of the main analyses of the sound data to find the precise moment of button failure will be presented.

6.1 Detecting the precise time of the button failure

The sound data was analysed with three different signal analysis techniques, that are, Time series analysis, Fourier Transform and Wavelet Transform, to find the exact moment of button failure of the right boom drill bit. The results of the above three signal processing techniques for the time arrays of both booms are working simultaneously will be presented. The results will be correlated by using 9 point moving average method and further supported by analysing the real time penetration rates.

6.1.1 Time Series analysis

Time series graphs created using OriginPro software were visually observed to identify the feasibility of detecting the differences between the two waveforms, that is, before the breakage and after the breakage of gauge button. Figure 24 illustrates a time series graph of sound signal before the button failure and the expanded view of the same graph. The sound waveform at the time of breakage and the expanded view of the same graph shows in Figure 25.

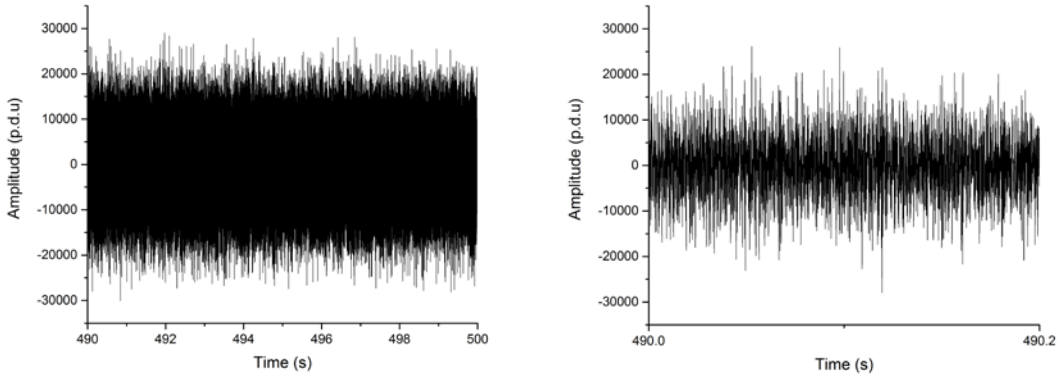

Figure 24: Time series graph- Before button failure (L) 490s – 500s (R) Expanded view

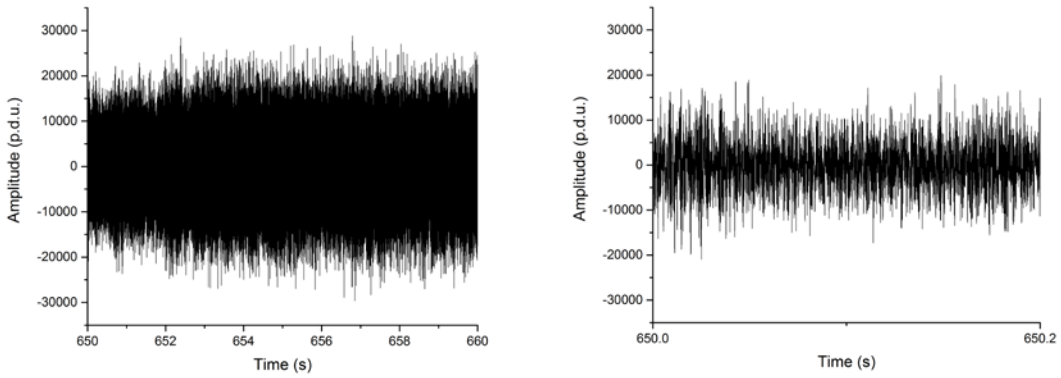

Figure 25: Time series graph at the time of breakage (L) 650s - 660s (R) Expanded view

As can be seen from Figure 24 and Figure 25, it is difficult to distinguish any abnormal feature at the time of button failure by visually analysing the time series graphs, even with the expanded views. Thus the statistical measures such as maximum, minimum, average and Standard Deviation (SD) values of the time series images were calculated. Table 6 represents those calculated values for two time arrays, which are before the button failure (300s to 580s) and after the button failure (650s to 900s), only when the both booms are working simultaneously.

Table 6: Statistical values of the Time series graph

Relative Index	Time range (s)	Minimum (p.d.u)	Minimum/10000	Maximum (p.d.u.)	Maximum/10000	Average	Standard Deviation
1	300-310	-30051	-3.0051	30157	3.0157	-0.70576	6579.51
2	310-320	-29699	-2.9699	28378	2.8378	0.21357	6584.13
3	320-330	-29656	-2.9656	28250	2.825	-0.3619	6649.99
4	330-340	-29948	-2.9948	29550	2.955	-0.58578	6609.01
5	340-350	-28534	-2.8534	28109	2.8109	-0.06429	6476.55
6	470-480	-30149	-3.0149	29370	2.937	-0.59929	6817.25
7	480-490	-30068	-3.0068	28915	2.8915	-0.29052	6729.93
8	490-500	-30059	-3.0059	28999	2.8999	-0.13562	6664.54
9	500-510	-29243	-2.9243	29279	2.9279	-0.8238	6597.06
10	510-520	-30446	-3.0446	29791	2.9791	-0.47007	6608.06
11	520-530	-29716	-2.9716	28036	2.8036	-0.36582	6765.87
12	530-540	-31596	-3.1596	30137	3.0137	-0.47343	6767.24
13	540-550	-29656	-2.9656	29829	2.9829	-1.13884	6754.83
14	550-560	-30071	-3.0071	29373	2.9373	-0.31067	6779.26
15	560-570	-28587	-2.8587	28050	2.805	-0.74502	6700.29
16	570-580	-29666	-2.9666	27351	2.7351	0.07216	6568.79
17	650-660	-29668	-2.9668	28822	2.8822	0.1675	6545.36
18	660-670	-29461	-2.9461	30085	3.0085	-0.63331	6639.28
19	670-680	-28974	-2.8974	28470	2.847	-0.53912	6636.44
20	680-690	-29965	-2.9965	29062	2.9062	-0.43803	6658.97
21	690-700	-29538	-2.9538	28630	2.863	-0.90697	6681.55
22	700-710	-29456	-2.9456	28902	2.8902	-0.4968	6699.25
23	710-720	-30437	-3.0437	29943	2.9943	-0.15679	6754.38
24	720-730	-30194	-3.0194	28284	2.8284	-0.43105	6845.51
25	840-850	-30372	-3.0372	28721	2.8721	-0.38235	6661.6
26	850-860	-28920	-2.892	28269	2.8269	-0.60037	6568.75
27	860-870	-28943	-2.8943	28104	2.8104	-0.34723	6495.08
28	870-880	-29329	-2.9329	26524	2.6524	-0.42268	6506.02
29	880-890	-29008	-2.9008	28146	2.8146	-0.20941	6631.75
30	890-900	-30981	-3.0981	29501	2.9501	-0.13478	6724.42

Figure 26 illustrates the variation of minimum, maximum and average values with the above time intervals. As it can be seen from the graph the minimum value varies within the range of -28500 p.d.u. to -31600 p.d.u. and maximum values varies within 26500 p.d.u. to 30200 p.d.u without any significant abnormal point or a trend to identify the breakage of the button. The average value of the time series graphs fluctuates between -1.139 and 0.214. A significant trend in the variation of the average amplitude cannot be identified by analysing the graph before and after the button failure.

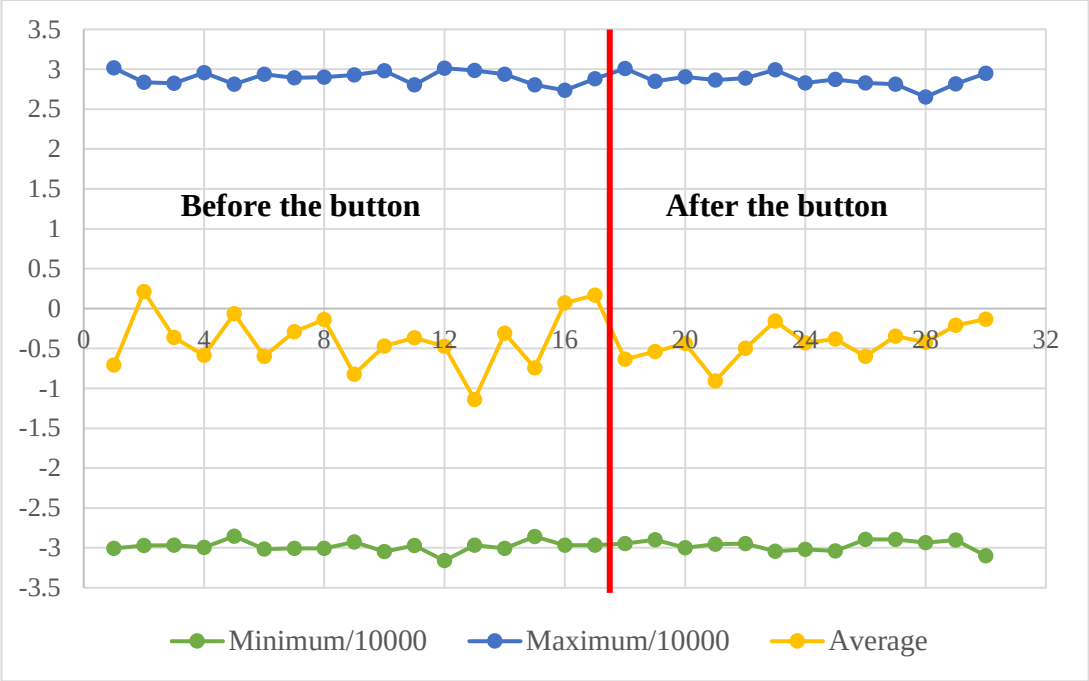

Figure 26: Variation of Minimum, Maximum and Average with time intervals

The standard deviation of the amplitude values of the sound wave fluctuates between 6400 to 6900 units. Figure 27 shows the changes in standard deviation and average amplitude with the above time intervals. Even with the changes of the average amplitude, the fluctuations of the standard deviation is considerably less. A visible variation which can be used to identify the precise moment of button failure cannot be detected, by analysing the changes of the Standard deviation of the Time series graphs. Thus it is obvious that the time series analysis cannot be used to identify the button failure of a drill bit because the polynomial signals could disguise the weak singularity points.

Fourier Transform analysis was conducted to identify the precise moment of button failure as it was not viable through the time series analysis.

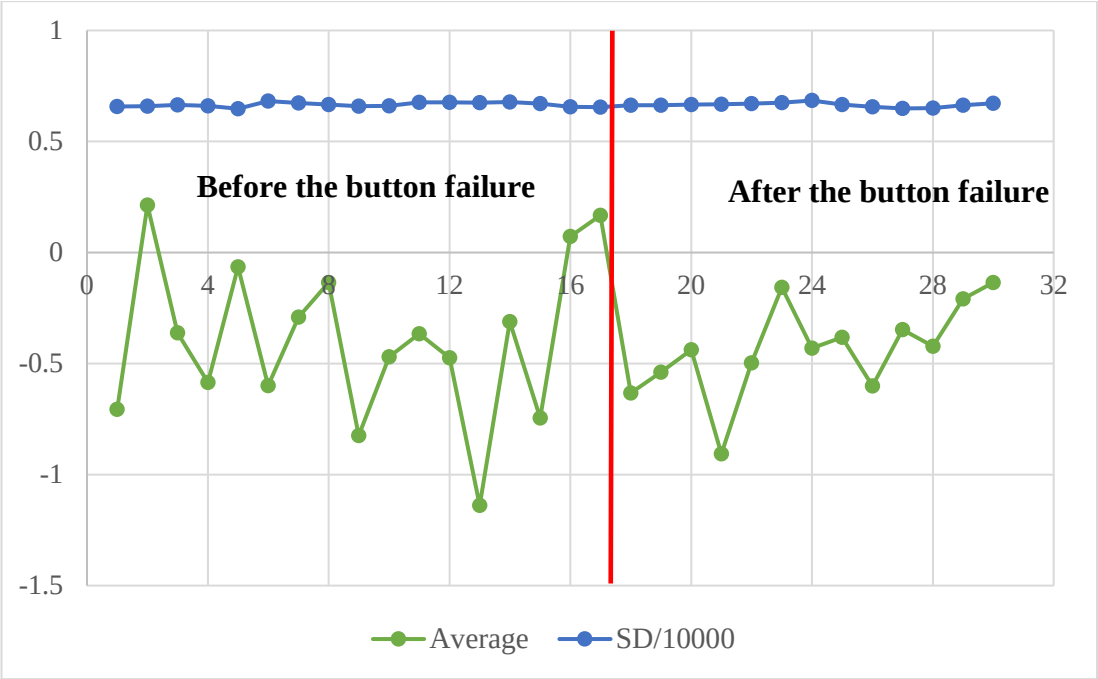

Figure 27: Variation of Standard Deviation and Average with the time intervals

6.1.2 Fourier Transform Analysis

Fourier Transform converted the time domain sound data in to its frequency components. The frequency graphs were created using OriginPro software and analysis was done for the time intervals, where both booms were working simultaneously. The graphs were visually analysed to compare with each other to detect any abnormalities which can be related to the button failure of the drill bit.

The following section presents a visual comparison of few frequency graphs for 10s time intervals, while both booms are working simultaneously.

6.1.2.1 Visual comparison between frequency graphs before the button failure

Figure 28 illustrates the frequency graphs for the time intervals of 490s – 500s and 500s – 510s and Figure 29 shows he frequency graphs for the time intervals of 510s – 520s and 520s – 530s. There is a dissimilarity in the frequency range of 0 Hz to 4 kHz, which is highly influenced by the surrounding sounds such as sound of the engine and motors of the drill rig. However, from 4 kHz onwards the variation of frequency is almost identical. All the other time intervals when both booms are working simultaneously, shows the same pattern of frequency variation, before the failure of the button of the right boom drill bit.

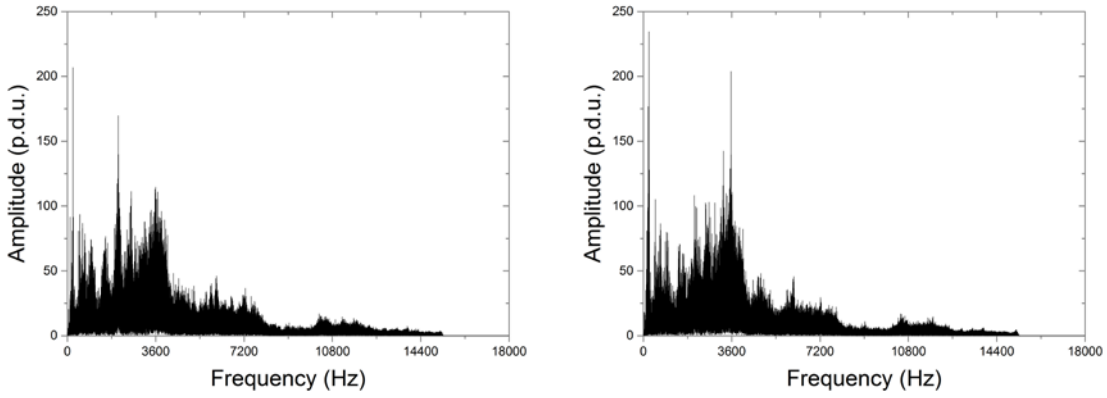

Figure 28: Frequency graphs (L) 490s to 500s (R) 500s to 510s

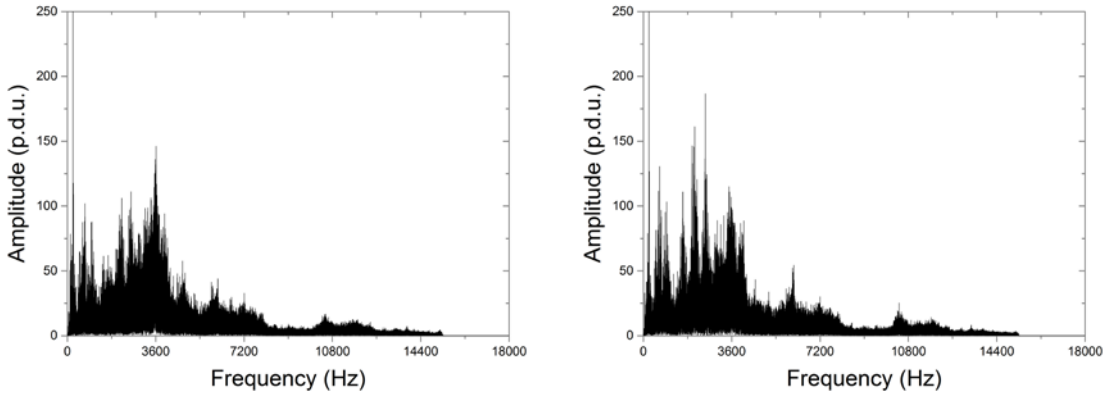

Figure 29: Frequency graphs (L) 510s to 520s (R) 520s to 530s

6.1.2.2 Visual comparison between frequency graphs after the button failure

The frequency graphs for the time intervals of 680s – 690s and 690s – 700s shows in Figure 30. Figure 31 illustrates the frequency graphs for the time intervals of 700s – 710s and 710s – 720s. As similar to the frequency graphs before the button failure, there is an unevenness variation in amplitudes, until the 4 kHz frequency limit, in the frequency graphs after the button failure. After the 4 kHz frequency the variation pattern is virtually identical. This variation pattern can be seen in all the other frequency graphs after the button failure, while both booms are working simultaneously.

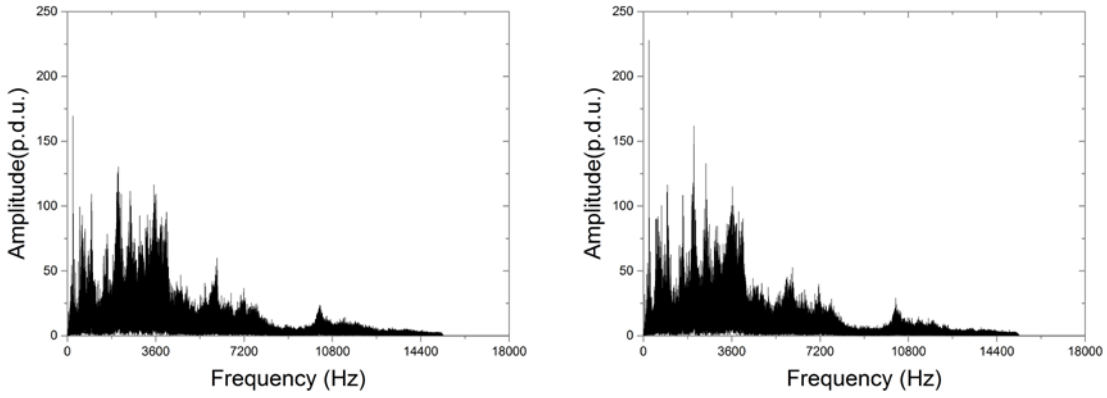

Figure 30: Frequency graphs (L) 680s to 690s (R) 690s to 700s

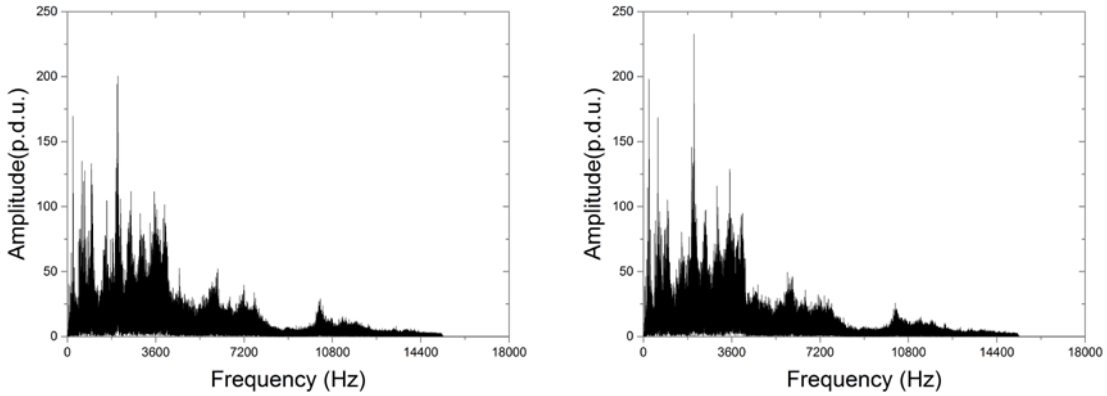

Figure 31: Frequency graphs (L) 700s to 710s (R) 710s to 720s

6.1.2.3 Visual comparison between Frequency graphs before and after the button failure

Figure 32 illustrates a frequency graphs before the button failure (550s – 560s) and after the button failure (680s – 690s), while the both booms are working simultaneously. There is a slight escalation in amplitudes in the frequency range of 5.7 kHz to 6.2 kHz. The trend of escalation begins at 660s to 670s time period and it remains after that for the frequency graphs, where both booms are working simultaneously. Thus the frequency range of 4.2 kHz to 8.2 kHz was statistically analysed to find the trend and to narrow down the time period which the button failure occurred.

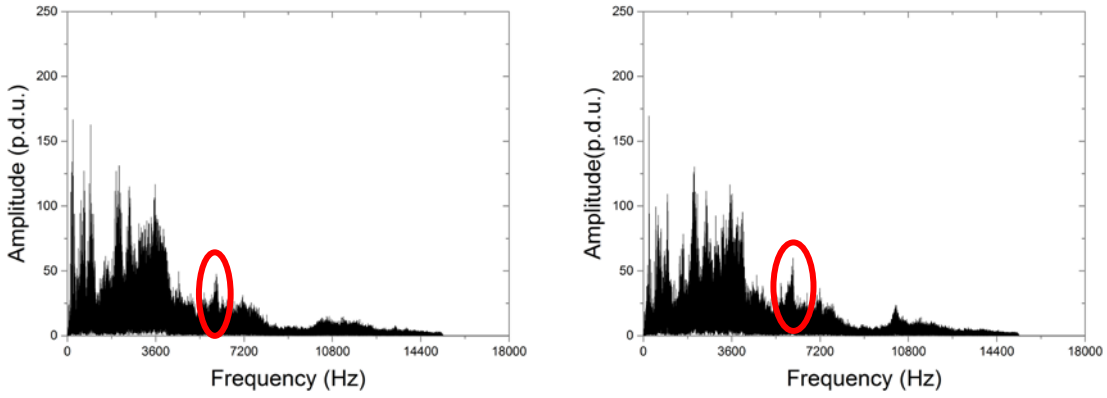

Figure 32: Frequency Graphs (L) Before failure - 550s to 560s (R) After failure - 680s to 690s

6.1.2.4 Statistical comparison of frequency graphs before and after the button failure

The frequency range of 4.2 kHz to 8.2 kHz was divided in to 500 Hz frequency groups and the integrated amplitude over that 500 Hz range was calculated for the 10s time intervals, where both booms are working simultaneously. Table 7 illustrates the integrated amplitude values for the 500 Hz frequency groups from 4.2 kHz to 6.2 kHz. Integrated amplitude values of 500 Hz frequency groups from 6.2 kHz to 8.2 kHz frequency range shows in Table 8.

Table 7: Integrated Amplitude (4.2 kHz - 6.2 kHz)

Relative Index	Real time (s)	Integrated Amplitude (4.2-4.7 kHz)	Integrated Amplitude (4.7-5.2 kHz)	Integrated Amplitude (5.2-5.7 kHz)	Integrated Amplitude (5.7-6.2 kHz)
1	130-140	5784.82	5175.81	4177.47	5724.13
2	140-150	5804.82	5257.81	4338.12	5650.64
3	150-160	5924.91	5209.01	4235.42	5694.06
4	160-170	6368.51	5575.29	3984.02	4936.59
5	170-180	6591.31	5595.67	3958.6	4968.2
6	290-300	6483.02	5395.61	4557.48	6065.49
7	300-310	5484.36	4951.88	4049.39	5953.83
8	310-320	6022.32	5529.5	4287.43	5539.22
9	320-330	6231.96	5504.07	4141.46	5383.29
10	330-340	6325.2	5595.67	4007.71	5129.73
11	490-500	5970.93	5323.1	4245.87	6009.57
12	500-510	6103.72	5949.74	3952.49	5409.66
13	510-520	6422.02	5648.24	3881.82	5630.66
14	520-530	5357.84	4605.58	3865.59	5742.35
15	530-540	5204.52	4403.03	4045.15	5945.88
16	540-550	5340.26	4485.06	3957.71	5783.77
17	550-560	5611.72	4690.24	4206.09	5682.24
18	560-570	5546.73	4617.88	4039.67	5789.7
19	650-660	6675.93	5686.4	4664.9	5866.86
20	660-670	6525.29	5484.89	4440.66	6167.22
21	670-680	6375.88	5730.94	4265.15	6635.18
22	680-690	6460.15	5221.18	4522.14	6690.96
23	690-700	6253.17	5266.99	4589.05	6911.89
24	700-710	5850.87	4753.14	4631.49	6655.37
25	710-720	5764.18	4861.18	4480.01	6286.89
26	720-730	5467.83	4422.57	4167.39	6249.14
27	840-850	6628.97	5134.1	4783.77	7055.49
28	850-860	6263.44	5415.3	4405.4	6917.86
29	860-870	6162.06	5049.18	4463.96	6764.26
30	870-880	6070.06	4656.19	4365.04	6654.69
31	880-890	5897.69	4668.36	4107.96	6606.08
32	890-900	5415.81	4241.38	3967.28	6586.32
33	900-910	5486.13	4354	3874.67	6719.25
34	1000-1010	6734.96	5350.2	4585.61	6818.14
35	1010-1020	6741.96	4972.86	4389.73	6581.85
36	1020-1030	6753.32	5159.68	4502.52	6577.87
37	1030-1040	6627.39	5127.15	4595.52	6786.26
38	1040-1050	6176.64	4989.51	4569.32	6920.71

Table 8: Integrated Amplitude (6.2 kHz - 8.2 kHz)

Relative Index	Real time (s)	Integrated Amplitude (6.2-6.7 kHz)	Integrated Amplitude (6.7-7.2 kHz)	Integrated Amplitude (7.2-7.7 kHz)	Integrated Amplitude (7.7-8.2 kHz)
1	130-140	4564.15	4009.93	3855.71	2603.26
2	140-150	4662.9	4186.03	4046.67	2530.27
3	150-160	4075.46	4045.51	4277.55	2591.87
4	160-170	4154.66	4035.3	4050.62	2323.02
5	170-180	4213.7	4324.34	3975.28	2328.72
6	290-300	4802.6	4398.4	4059.39	2536.11
7	300-310	4262.25	3966.14	4038.3	2481.77
8	310-320	4332.14	3907.25	3661.32	2348.1
9	320-330	4442.84	4063.17	3916.47	2306.76
10	330-340	4635.14	4411.32	3764.99	2132.47
11	490-500	4387.23	4347.78	4211.77	2659.98
12	500-510	4181.69	3919.11	3663.86	2424.41
13	510-520	4227.6	3981.88	3786.66	2419.37
14	520-530	4035.03	3802.94	3601.83	2431.05
15	530-540	4011.61	3820.36	3663.02	2487.54
16	540-550	4423.95	3944.2	3660.87	2499.88
17	550-560	4364.13	4431.69	3973.78	2540.4
18	560-570	5016.94	4940.07	3987.34	2381.26
19	650-660	4301.64	4137.57	3645.31	2604.41
20	660-670	4179.54	4329.68	4098.05	2619.91
21	670-680	4435.42	4433.98	4048.59	2607.29
22	680-690	4359.05	4357.24	4071.44	2697.26
23	690-700	4625.8	4481.64	4266.54	2761.82
24	700-710	4572.85	4478.99	4377.67	2752.96
25	710-720	4644.21	4198.75	4240.9	2656.05
26	720-730	4440.5	4363.71	4103.03	2358.39
27	840-850	4657.93	4368.99	3881.73	2570.89
28	850-860	4461.53	4451.78	4232.53	2743.61
29	860-870	4916.4	4788.93	4199.23	2839.5
30	870-880	4958.41	4730.77	4179.29	2772.68
31	880-890	4206.32	4430.52	4150.09	2786.1
32	890-900	4036.76	4296.09	4288.64	2736.86
33	900-910	4244.61	4416.56	4143.89	2560.22
34	1000-1010	4475.37	4588.24	4224.56	2655.71
35	1010-1020	4588.9	4536.56	4277.59	2925.49
36	1020-1030	4607.42	4602.38	4374.22	2877.85
37	1030-1040	4788.13	4619.62	4534.06	2753.03
38	1040-1050	4383.5	4732.65	4400.13	2823.8

The variation of integrated amplitudes of the frequency range of 4.2 kHz to 8.2 kHz over the time period, when the both booms are working simultaneously, illustrates in Figure 33, Figure 34, Figure 35 and Figure 36 respectively. As can be seen in Figure 34, the integrated amplitude for the frequency range of 5.7 kHz to 6.2 kHz indicates a significant escalation after 650s – 660s time interval. Before the 650s – 660s time interval, the integrated amplitude varies between the values of 5500 to 6000 and after 660s – 670s time interval, it varies between the values of 6500 to 7000.

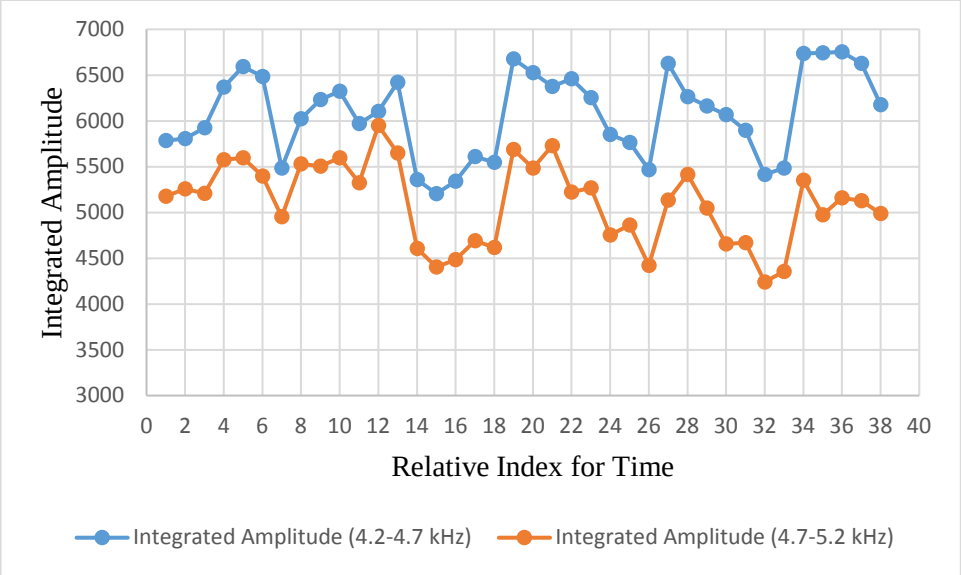

Figure 33: Variation of Integrated amplitude (4.2 kHz-4.7 kHz and 4.7 kHz-5.2 KHz)

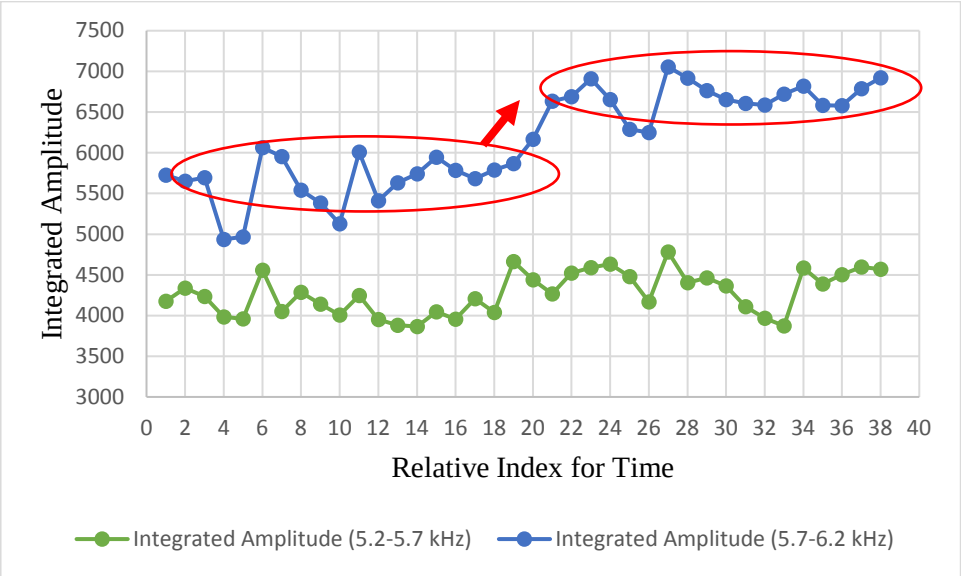

Figure 34: Variation of Integrated amplitude (5.2 kHz-5.7 kHz and 5.7 kHz-6.2 kHz)

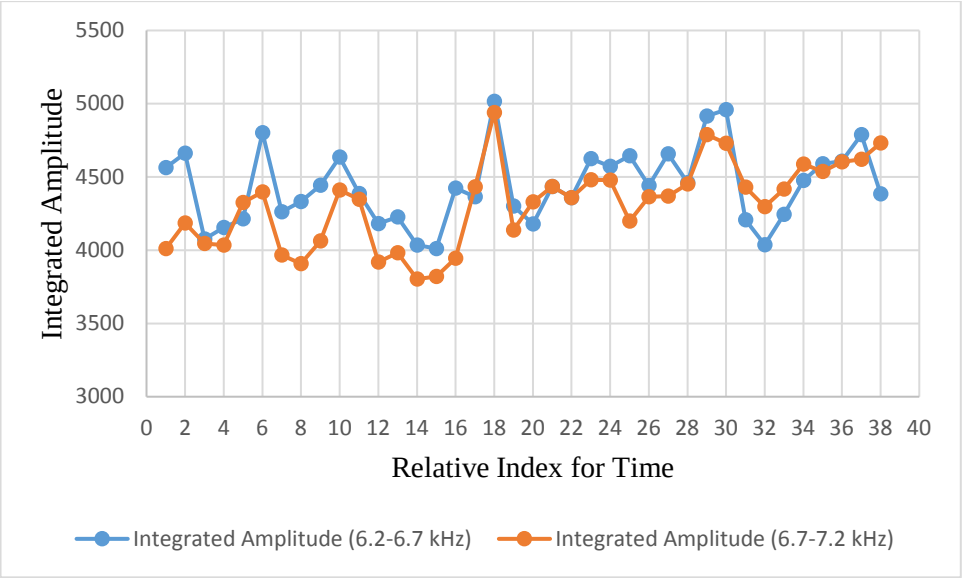

Figure 35: Variation of Integrated amplitude (6.2 kHz-6.7 kHz and 6.7 kHz-7.2 kHz)

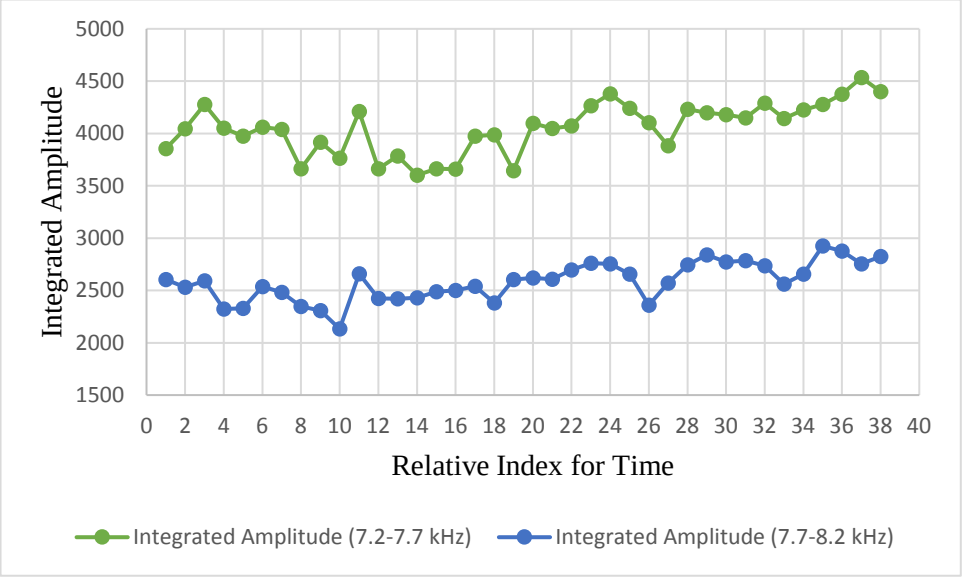

Figure 36: Variation of Integrated Amplitude (7.2 kHz-7.7 kHz and 7.7 kHz-8.2 kHz)

The variation of integrated amplitude for the other frequency ranges do not illustrates a clear trend of deviation, which can be related to the failure of button. Thus the time interval which is related to the failure of the button of the right boom drill bit was narrowed down to 650s to 680s. However, the exact moment of button failure was not detected because of the incapability of FFT in detecting a singularity point in a wide range of frequency distribution. Thus the Wavelet Transform was used to detect the exact moment of button failure.

6.1.3 Wavelet Transform Analysis

The time domain sound data was converted into the frequency domain data using Wavelet Transform, which illustrates the changes of the intensity of the waveform with time and frequency. The time period of 650s to 680s was divided in to 0.2s time intervals and time – frequency spectrum was created using GeoLab Analyser software.

6.1.3.1 Visual comparison of time – frequency spectrum

Time frequency graphs were visually observed and compared to find the high intensity point, which is related to the button failure of the right boom drill bit. Figure 37 illustrates a time – frequency spectrum of 650.0s to 650.2s, which is a normal drilling condition before the button failure occurred.

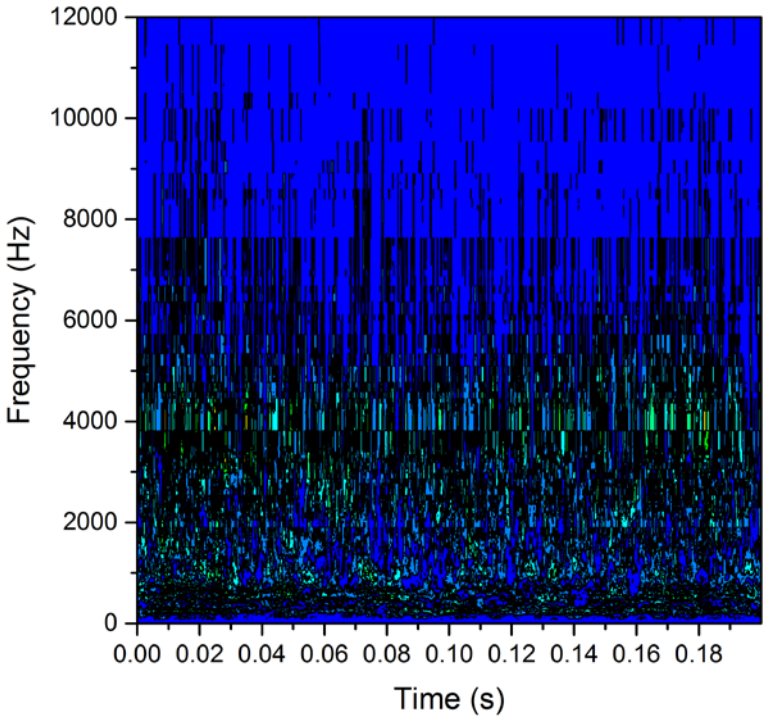

Figure 37: Time - Frequency spectrum of a normal drilling condition (650.0s - 650.2s)

The time – frequency spectrums at the time of button failure and after the button failure illustrates Figure 38 and Figure 39 respectively. A high intensity point can be seen in Figure 38, which is related to the time interval of 652.6s to 652.8s in comparison to all other wavelet graphs. The high intensity point can be seen at around 500 Hz frequency range. Figure 40 illustrates the time - frequency spectrum of 0 Hz to 700 Hz at the time of button breakage.

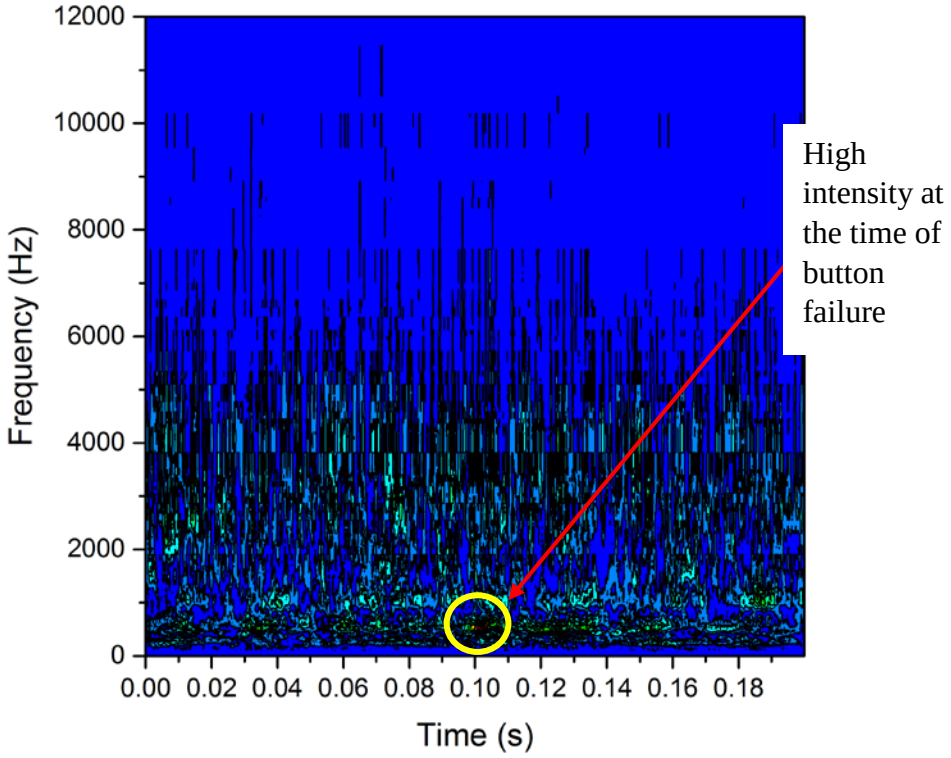

Figure 38: Time - Frequency spectrum at the time of button failure (652.6s - 652.8s)

In signal processing, singularity is considered as a sudden change of signal's value to a different amount, which may occurred due to a tool breakage of chipping of material. Weak singularity points of a signal can be disguised by the polynomial trends of that signal. In comparison to some other signal processing techniques, Wavelet transform can eliminate those polynomial trends to distinguish the weak singularity points. Thus, high intensity point in a time – frequency spectrum can be correlated to a time of button failure. The typical maximum intensity of the frequency range of 500 Hz to 600 Hz, varies around 0.5 to 0.6, while at 652.8s it increased approximately up to 0.9. Thus it is obvious that the peak point around 500 Hz to 600 Hz in Figure 40 is related to the button failure of the right boom drill bit, which occurred at 652.8s. Further this results were correlated to the average intensity between the frequencies of 5.7 kHz to 6.2 kHz by analysing the wavelet matrix.

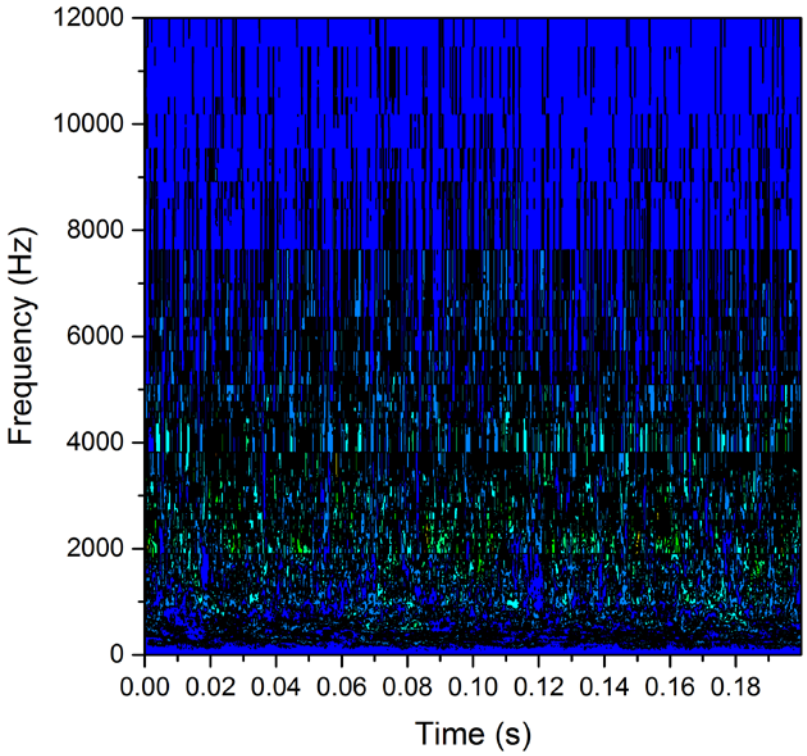

Figure 39: Time - Frequency spectrum after the button failure (658.8s - 659.0s)

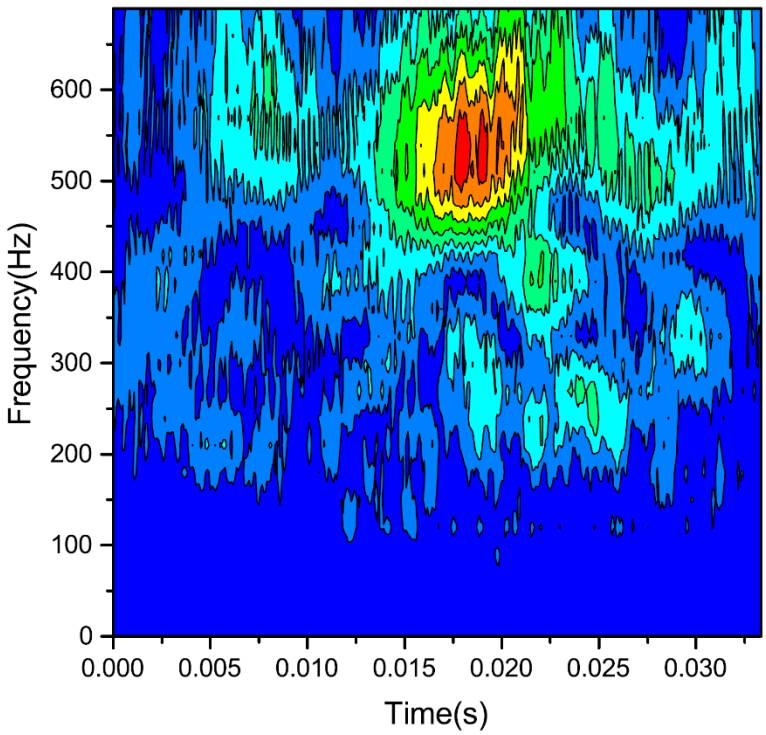

Figure 40: Time - Frequency Spectrum at the time of breakage (expanded - 0 Hz to 700 Hz)

6.1.3.2 Statistical analysis of Wavelet matrix data

Two predefined time arrays were defined as described in data analysis procedure section and maximum intensity and the average intensity were calculated for the frequency ranges 500 Hz to 600 Hz and 5.7 kHz to 6.2 kHz respectively. For all those values 9 point moving average was calculated to identify the trends. Table 9 illustrates the 9 point moving average values of maximum intensity and average intensity before the button failure, for the above mentioned respective frequency ranges. Nine point moving average values of maximum and average intensity after the button failure illustrates in Table 10.

Table 9: Average and Maximum intensity - Before the button failure (491.0s - 499.2s)

Relative Index for Time	Time(s)	Average intensity (5.7-6.2 kHz)	Maximum intensity (500-600Hz)
1	491	0.927459111	0.559361689
2	491.2	0.934945111	0.567893833
3	491.4	0.938207111	0.563343033
4	491.6	0.941153556	0.557292733
5	491.8	0.952878444	0.569417511
6	492	0.964273667	0.568336533
7	492.2	0.975588444	0.576056822
8	492.4	0.983527222	0.569027233
9	492.6	0.985524444	0.561508978
10	492.8	0.987777556	0.566920644
11	493	0.980481444	0.570807122
12	493.2	0.988542556	0.574914211
13	493.4	0.990931556	0.566836278
14	493.6	0.989959	0.553808233
15	493.8	0.985949111	0.549677222
16	494	0.981018333	0.5353087
17	494.2	0.975792222	0.532715222
18	494.4	0.970976667	0.529865511
19	494.6	0.965172889	0.534145922
20	494.8	0.974287333	0.526291989
21	495	0.974924444	0.528616022
22	495.2	0.970512667	0.543852622
23	495.4	0.968262111	0.541838356
24	495.6	0.975725222	0.5457798
25	495.8	0.975113556	0.553109233
26	496	0.977646	0.545682022
27	496.2	0.983358444	0.545377122
28	496.4	0.984932889	0.537968089
29	496.6	0.974294778	0.534858167
30	496.8	0.965800556	0.519706111
31	497	0.969491	0.499069889
32	497.2	0.965190556	0.501043956
33	497.4	0.962616667	0.499463878
34	497.6	0.963438111	0.497532911
35	497.8	0.965215111	0.501847589
36	498	0.964523667	0.5075785
37	498.2	0.963000111	0.500809533
38	498.4	0.967589556	0.487659478
39	498.6	0.962782222	0.5000373
40	498.8	0.960059778	0.503943467
41	499	0.959963333	0.507943089
42	499.2	0.952141111	0.502724133

Table 10: Average and Maximum intensity - After the button failure (650.0s - 658.6s)

Relative Index for Time	Time(s)	Average intensity (5.7 kHz-6.2 kHz)	Maximum intensity (500-600Hz)
43	650	0.762421222	0.582274433
44	650.2	0.766681667	0.579042267
45	650.4	0.764504556	0.576536311
46	650.6	0.761373111	0.583959133
47	650.8	0.750988	0.571391933
48	651	0.745541667	0.5846547
49	651.2	0.751771222	0.620140122
50	651.4	0.770775556	0.637504344
51	651.6	0.791890111	0.663557622
52	651.8	0.799013111	0.716300922
53	652	0.827014556	0.755840344
54	652.2	0.861824667	0.793031089
55	652.4	0.891076667	0.799709311
56	652.6	0.921422222	0.824954722
57	652.8	0.952593556	0.850278344
58	653	0.981479222	0.824746822
59	653.2	1.000953889	0.842393856
60	653.4	1.020433444	0.843720978
61	653.6	1.042188778	0.786948689
62	653.8	1.036428778	0.7581256
63	654	1.039759444	0.739551778
64	654.2	1.042535889	0.736684622
65	654.4	1.046791111	0.731888622
66	654.6	1.044309	0.706850433
67	654.8	1.039821889	0.7164016
68	655	1.032076333	0.689190111
69	655.2	1.026165556	0.683958444
70	655.4	1.020733889	0.689851656
71	655.6	1.025405444	0.698601633
72	655.8	1.022141889	0.707118144
73	656	1.010795111	0.712591667
74	656.2	1.006106778	0.731508289
75	656.4	1.011358556	0.721527222
76	656.6	1.010918556	0.726823956
77	656.8	1.013116444	0.719761322
78	657	1.010326778	0.706833567
79	657.2	1.021965556	0.688458789
80	657.4	1.022461111	0.649477744
81	657.6	1.016287556	0.614485767
82	657.8	1.013430889	0.576054867
83	658	1.014715333	0.517670311
84	658.2	1.022492667	0.491341178
85	658.4	1.028970444	0.457057822
86	658.6	1.02648	0.443853733

The variation of average and maximum intensity over the predefined time intervals illustrates in Figure 41. As can be seen in Figure 41, the maximum intensity between 500 Hz to 600 Hz frequency range reaches to a peak value of 0.85 at 652.8s. The singularity point at 652.8s correlates to the trend of average intensity variation between 5.7 kHz to 6.2 kHz frequency range. There is a significant escalation in average intensity after the button failure at 652.8s. Before the button failure average intensity retains around 0.9 to 1.0 and it increases up to 1.0 to 1.1 range after the button failure. Thus it is obvious that the button failure occurred at 652.8s and this is further evidence to the conclusions of visual observations of the time – frequency spectrums.

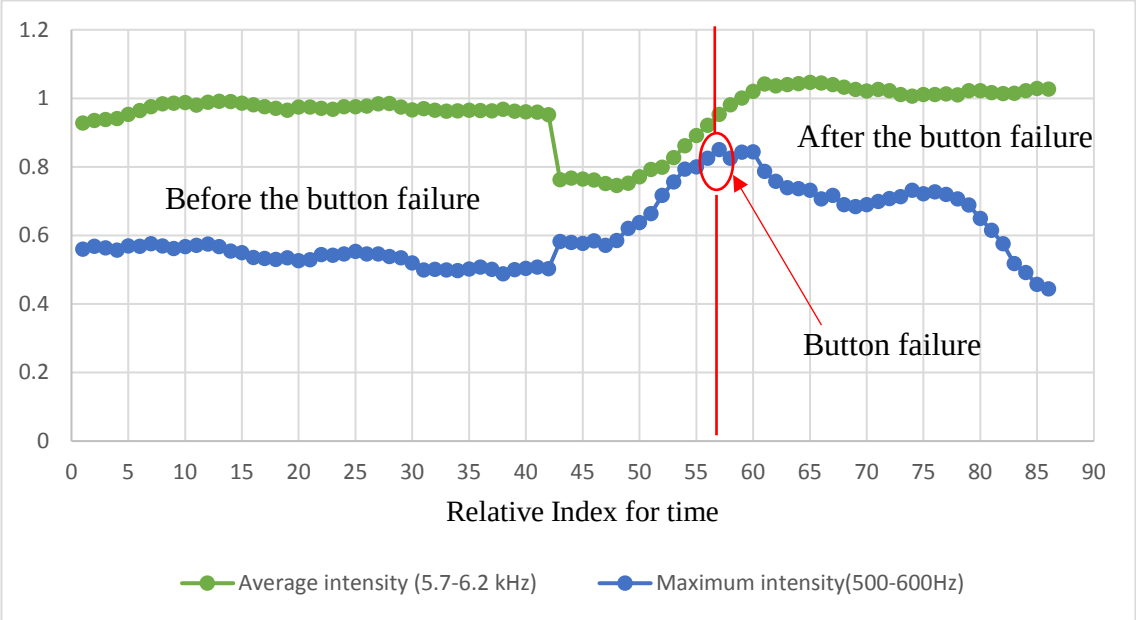

Figure 41: The variation of Average and Maximum intensity (Before and after the button failure)

6.1.4 Real time penetration rate analysis

Time conceded to drill each 4m hole were recorded by analysing the video data to correlate the penetration rate variation with the button failure of the drill bit. Table 11 illustrates the time conceded to drill each hole by using right boom and left boom separately. Figure 42 illustrates the variation of time conceded to drill each hole using the right boom and left boom. It can be seen that the penetration rate for the left boom retain to be almost consistent around 120s to 130s per 4m hole. However, the variation of penetration rates for the right boom indicates a gradual increase after the button failure at 652.8s. Average time conceded to drill a one hole using right boom retains

around 130s before the button failure, which increases up to 175s after the button failure.

Right boom bit button failure occurred at 652.8s and it can be seen that three holes were drilled using the right boom before the button failure. The average penetration rate before the button failure for the right boom drill bit is about 3.023 cm/s and it decreased to 2.28 cm/s, after the failure of the button. In comparison to the right boom average penetration rate for the left boom is 3.162 cm/s and retain to be constant over the time period.

Table 11: Penetration rates at real time drilling

Hole No	**Time(s) /hole (Right boom)**	**Average Penetration rate - right boom (cm/s)**	**Time(s)/hole (left boom)**	**Average penetration rate - left boom (cm/s)**
1	139		105	
2	125		113	
3	133	**3.023**	151	
4	141	**Button failure**	170	
5	143		131	
6	160		136	
7	170		109	
8	200		116	
9	178		103	
10	168		134	
11	188		109	
12	196		125	
13	189		110	
14	163		112	
15	162		134	
16	161		133	
17	203	**2.280**	138	
18	0		148	
19	0		132	
20	0		127	
21	0		121	**3.162**

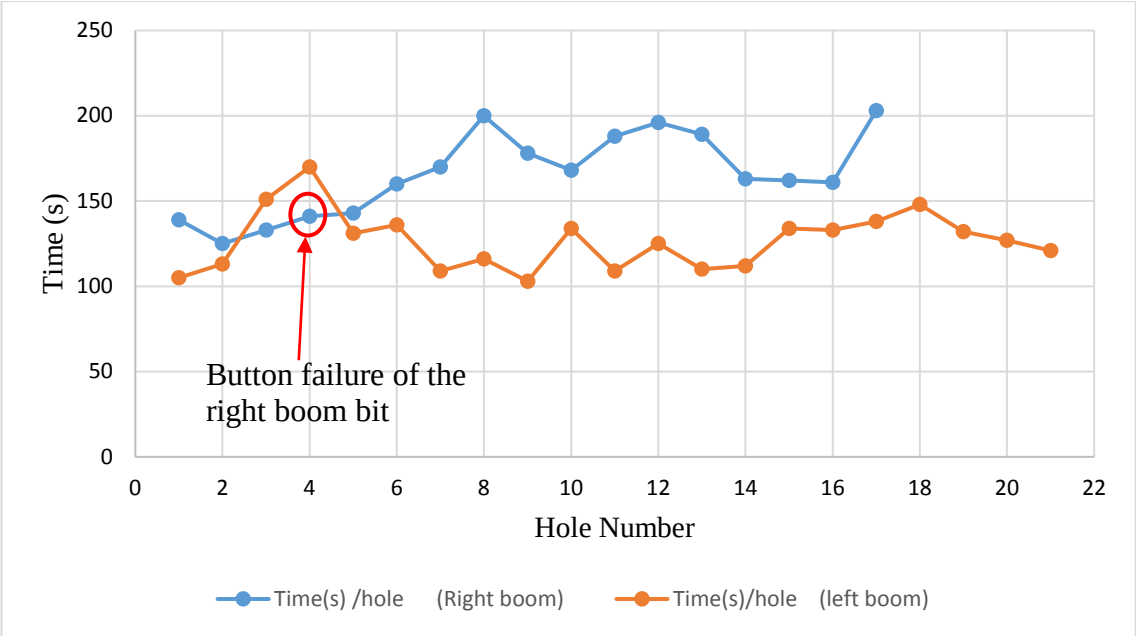

Figure 42: Variation of time conceded to drill each hole (Right boom and left boom)

The penetration rate in hard rock drilling is going to be decreased after button failures of drill bits. Thus the correlation of penetration rate variation before and after the button failure is further evidence to the button failure at 652.8s.

6.2 Summary

Time series analysis of the sound data cannot distinguish any abnormal points which can be related to the failure of the button of the drill bit, since the polynomial sound signal disguises the weak singularity points. After a comprehensive analysis of frequency graphs generated under the theory of Fourier Transform, a slight escalation of integrated amplitude can be seen in 5.7 kHz – 6.2 kHz frequency range after the 680s. Furthermore, the Fourier analysis narrows the time period, which the button failure occurred to 650 s – 680 s.

Wavelet analysis was used to generate the time – frequency spectrum of the above 30 s time period. Analysis of Time – frequency spectrum illustrates that the button failure occurred at 652.8 s, where a high intensity point can be seen. Moreover, the results were correlated with the statistical analysis of average intensity between 5.7 kHz – 6.2 kHz frequency range where, a significant escalation of average intensity can be seen after the button failure. Furthermore, the penetration rate analysis shows a decrease in penetration rate in right boom after the button failure, which is further evidence for the findings with Wavelet Transform.

CHAPTER 7. CONCLUSIONS AND RECOMMENDATIONS

The main objective of this research was to introduce a new reliable methodology to detect the precise moment of button failure of a drill bit during a real time drilling process. To accomplish the aforementioned objective, an experiment was conducted in an underground copper mine site in Queensland, Australia in collaboration with Mitsubishi Materials Corporation to acquire the sound data during a real time drilling process. The recorded sound data was then analysed with different waveform analysis techniques including, Time series Analysis, Fourier Transform and Wavelet Transform.

7.1 Conclusions

It is vital to detect the precise moment of button failure of a drill bit to avoid the further damage to the drill bit as well as to maintain a healthy penetration rate. Over the years, the detection of abnormalities in hard rock drilling including button failures, solely depended on the experience of the drill rig operators. However, it is subjective and susceptible to human errors. Thus, a more reliable method to detect the precise moment of button failure is desired.

In this research, the sound data which are collected during a real time drilling process was analysed with waveform analysis techniques to detect the precise moment of button failure of a drill bit.

The time series graphs were generated using the sound data acquired and the graphs were analysed visually and statistically to detect any abnormalities which can be related to the failure of the button. The results of the analysis indicates that, it is difficult to identify a singularity point which can be occurred at a time of button failure due to the disguise of the weak singularity points by the polynomial sound signals.

Fast Fourier Transform was used to generate the frequency spectrums of the time domain sound data. A robust analysis of frequency graphs showed variations of amplitudes in a selected frequency range, before and after the button failure. Although the results assisted to narrow the time range, which the button failure occurred, the Fourier Transform analysis cannot identify a peak singularity point in a wide range of frequency distribution.

Time – frequency spectrums were created using Wavelet transform to detect the exact moment of button failure of drill bit. High amplitude generated at the time of button failure was indicated by the high intensity point in time – frequency spectrum. Thus, the exact moment of button failure and the frequency range related to the failure can be identified by analysing the time – frequency spectrum of the sound data. Hence, the results demonstrates that the sound generated during a hard rock drilling process can be used to detect the exact moment of button failure by analysing the sound data with Wavelet transform. It also shows that the Wavelet transform is a much superior signal processing technique for singularity detection in comparison to other two methods.

7.2 Recommendations for Future Research

A number of recommendations can be made in regards to the future research related to the early diagnosis of rock tool failures during a hard rock drilling process.

The research was conducted for a single rock type and drilling conditions. Thus, it is important to conduct further research under different drilling and rock conditions to provide further insight in to the rock-bit interactions using sound analysis. Moreover, it is recommended to conduct a similar kind of analysis by collecting two types of data such as, sound and vibration for a same drilling process for verification of the findings before a practical invention. Furthermore, the experiment can be expanded to detect the failures of other rock tools including, drill rod and shank adapter.

REFERENCES

Adewusi, S., & Al-Bedoor, B. (2001). Wavelet analysis of vibration signals of an overhang rotor with a propagating transverse crack. *Journal of Sound and Vibration, 246*(5), 777-793.

Barry, N. W., Raghu, N. S., & Gexin, S. (1992). Rock fracture mechanics principles design and applications: ELSEVIER, Amsterdam-London-New York-Tokyo.

Bisu, C. F., Zapciu, M., Cahuc, O., Gérard, A., & Anica, M. (2012). Envelope dynamic analysis: a new approach for milling process monitoring. *The International Journal of Advanced Manufacturing Technology, 62*(5-8), 471-486.

Brennan, M., Chen, M., & Reynolds, A. (1997). Use of vibration measurements to detect local tooth defects in gears. *SV Sound and vibration, 31*(11), 12-17.

Chen, X., & Li, B. (2006). Acoustic emission method for tool condition monitoring based on wavelet analysis. *The International Journal of Advanced Manufacturing Technology, 33*(9), 968-976. doi: 10.1007/s00170-006-0523-5

Cheng, K. (2008). *Machining dynamics: fundamentals, applications and practices*: Springer Science & Business Media.

Choi, Y., Narayanaswami, R., & Chandra, A. (2004). Tool wear monitoring in ramp cuts in end milling using the wavelet transform. *The International Journal of Advanced Manufacturing Technology, 23*(5-6), 419-428.

Cooley, J. W., & Tukey, J. W. (1965). An algorithm for the machine calculation of complex Fourier series. *Mathematics of computation, 19*(90), 297-301.

Dimla, D. E. (2002). The correlation of vibration signal features to cutting tool wear in a metal turning operation. *The International Journal of Advanced Manufacturing Technology, 19*(10), 705-713.

Dornfeld, D., & Cai, H. G. (1984). An investigation of grinding and wheel loading using acoustic emission. *Journal of Engineering for Industry, 106*(1), 28-33.

El-Wardany, T. I., Gao, D., & Elbestawi, M. A. (1996). Tool condition monitoring in drilling using vibration signature analysis. *International Journal of Machine Tools and Manufacture, 36*(6), 687-711. doi: http://dx.doi.org/10.1016/0890-6955(95)00058-5

Fu, J., Troy, C., & Mori, K. (1996). The prediction of small drill bit breakage by wavelet based joint time-scale analysis. *CIRP Proceedings--Manufacturing System, 385*(389).

Furutani, K., Ohguro, N., Hieu, N. T., & Nakamura, T. (2002). In-process measurement of topography change of grinding wheel by using hydrodynamic pressure. *International Journal of Machine Tools and Manufacture, 42*(13), 1447-1453.

Gong, W., Obikawa, T., & Shirakashi, T. (1997). Monitoring of tool wear states in turning based on wavelet analysis. *JSME international journal. Series C, dynamics, control, robotics, design and manufacturing, 40*(3), 447-453.

Gradl, C., Eustes, A. W., & Thonhauser, G. (2011). An Analysis of Noise Characteristics of Drill Bits. *Journal of Energy Resources Technology, 134*(1), 013103-013103. doi: 10.1115/1.4005324

Han, X., & Wu, T. (2013). Analysis of acoustic emission in precision and high-efficiency grinding technology. *The International Journal of Advanced Manufacturing Technology, 67*(9-12), 1997-2006.

Hosokawa, A., Mashimo, K., Yamada, K., & Ueda, T. (2004). Evaluation of grinding wheel surface by means of grinding sound discrimination. *JSME International Journal Series C Mechanical Systems, Machine Elements and Manufacturing, 47*(1), 52-58.

Huang, S., & Wang, Z. (1997). The mechanics of diamond core drilling of rocks. *International Journal of Rock Mechanics and Mining Sciences, 34*(3), 134. e131-134. e114.

Inasaki, I. (1991). Monitoring and optimization of internal grinding process. *CIRP Annals-Manufacturing Technology, 40*(1), 359-362.

Inasaki, I., & Okamura, K. (1985). Monitoring of dressing and grinding processes with acoustic emission signals. *CIRP Annals-Manufacturing Technology, 34*(1), 277-280.

Iwata, K., & Moriwaki, T. (1977). An application of acoustic emission measurement to in-process sensing of tool wear. *Annals of the CIRP, 26*(1), 21-26.

Kannatey-Asibu, E., & Dornfeld, D. (1982). A study of tool wear using statistical analysis of metal-cutting acoustic emission. *Wear, 76*(2), 247-261.

Karakus, M., & Perez, S. (2014). Acoustic emission analysis for rock–bit interactions in impregnated diamond core drilling. *International Journal of Rock Mechanics and Mining Sciences, 68*(0), 36-43. doi: http://dx.doi.org/10.1016/j.ijrmms.2014.02.009

Kuljanic, E., Totis, G., & Sortino, M. (2009). Development of an intelligent multisensor chatter detection system in milling. *Mechanical Systems and Signal Processing, 23*(5), 1704-1718.

Kumar, B. R., Vardhan, H., & Govindaraj, M. (2011). Sound level produced during rock drilling vis-à-vis rock properties. *Engineering Geology, 123*(4), 333-337. doi: http://dx.doi.org/10.1016/j.enggeo.2011.09.009

Lan, M., & Dornfeld, D. (1982). *Experimental studies of tool wear via acoustic emission analysis.* Paper presented at the Proceedings of the 10th North American Manufacturing Research Conference.

Lee, D. T., & Yamamoto, A. (1994). Wavelet analysis: theory and applications. *Hewlett Packard journal, 45*, 44-44.

Li, S., & Li, S. (1990). Acoustic emission analysis for bearing condition monitoring. *co DTIC*, 249.

Li, X. (2002). A brief review: acoustic emission method for tool wear monitoring during turning. *International Journal of Machine Tools and Manufacture, 42*(2), 157-165. doi: http://dx.doi.org/10.1016/S0890-6955(01)00108-0

Li, X., Dong, S., & Yuan, Z. (1999). Discrete wavelet transform for tool breakage monitoring. *International Journal of Machine Tools and Manufacture, 39*(12), 1935-1944.

Liang, S., & Dornfeld, D. (1989). Tool wear detection using time series analysis of acoustic emission. *Journal of Engineering for Industry, 111*(3), 199-205.

Lin, J., & Qu, L. (2000). FEATURE EXTRACTION BASED ON MORLET WAVELET AND ITS APPLICATION FOR MECHANICAL FAULT DIAGNOSIS. *Journal of Sound and Vibration, 234*(1), 135-148. doi: http://dx.doi.org/10.1006/jsvi.2000.2864

Liu, B., & Ling, S.-F. (1999). On the selection of informative wavelets for machinery diagnosis. *Mechanical Systems and Signal Processing, 13*(1), 145-162.

Liu, B., Ling, S.-F., & Meng, Q. (1997). Machinery diagnosis based on wavelet packets. *Journal of vibration and control, 3*(1), 5-17.

Lu, C.-J., & Hsu, Y.-T. (2000). Application of wavelet transform to structural damage detection. *Shock and Vibration Digest, 32*(1), 50.

Lu, M.-C., & Kannatey-Asibu, E. (2002). Analysis of sound signal generation due to flank wear in turning. *Journal of Manufacturing Science and Engineering, 124*(4), 799-808.

Lu, M.-C., & Wan, B.-S. (2013). Study of high-frequency sound signals for tool wear monitoring in micromilling. *The International Journal of Advanced Manufacturing Technology, 66*(9-12), 1785-1792.

Mallat, S., & Hwang, W. L. (1992). Singularity detection and processing with wavelets. *Information Theory, IEEE Transactions on, 38*(2), 617-643.

Mallat, S. G. (1989). A theory for multiresolution signal decomposition: the wavelet representation. *Pattern Analysis and Machine Intelligence, IEEE Transactions on, 11*(7), 674-693.

Mitsubishi Rock Tools. Retrieved Accessed on 27th July 2015, from http://www.creightonrock.com/images/Mitsubishi_rt01a.pdf

Mokbel, A. A., & Maksoud, T. (2000). Monitoring of the condition of diamond grinding wheels using acoustic emission technique. *Journal of materials processing technology, 101*(1), 292-297.

Momoh, J. A., & Dias, L. G. (1996). Solar dynamic power system fault diagnosis.

Momoh, J. A., Oliver Jr, W. E., & Dolce, J. L. (1995). *Comparison of feature extractors on DC power system faults for improving ANN fault diagnosis accuracy*. Paper presented at the Systems, Man and Cybernetics, 1995. Intelligent Systems for the 21st Century., IEEE International Conference on.

Mori, K., Kasashima, N., Fu, J., & Muto, K. (1999). Prediction of small drill bit breakage by wavelet transforms and linear discriminant functions. *International Journal of Machine Tools and Manufacture, 39*(9), 1471-1484.

Moriwaki, T., & Okushima, K. (1980). Detection for cutting tool fracture by acoustic emission measurement. *CIRP Annals-Manufacturing Technology, 29*(1), 35-40.

Morlet, J., Arens, G., Fourgeau, E., & Glard, D. (1982). Wave propagation and sampling theory-Part I: Complex signal and scattering in multilayered media. *Geophysics, 47*(2), 203-221.

Nagayama, M., Kawamura, Y., & Ujihira, M. (2006). Study on the Detection of Misfiring Cylinder in a Heavy Machinery Multi-Cylinder Diesel Engine under the State of Rotational Fluctuation.

Newland, D. (1995). *Progress in the application of wavelet theory to vibration analysis.* Paper presented at the Proceedings of ASME 15th Biennial Conference on Mechanical Vibration and Noise, Boston.

Newland, D. E. (1994). Wavelet analysis of vibration: part 1—theory. *Journal of vibration and acoustics*, *116*(4), 409-416.

Pan, C., & Dornfeld, D. (1986). Modeling the Diamond-Turning Process with Acoustic Emission for Monitoring Applications. *Proc. 14th NAMRC, SME*, 257-265.

Paone, J., & Bruce, W. E. (1963). *Drillability studies: diamond drilling* (Vol. 6324): Bureau of Mines.

Paone, J., Bruce, W. E., & Virciglio, P. R. (1966). *Drillability studies: statistical regression analysis of diamond drilling*: US Dept. of the Interior, Bureau of Mines.

Peng, Z., & Chu, F. (2004). Application of the wavelet transform in machine condition monitoring and fault diagnostics: a review with bibliography. *Mechanical Systems and Signal Processing*, *18*(2), 199-221.

Peter, W. T., Peng, Y., & Yam, R. (2001). Wavelet analysis and envelope detection for rolling element bearing fault diagnosis—their effectiveness and flexibilities. *Journal of vibration and acoustics*, *123*(3), 303-310.

Peter, W. T., Yang, W.-x., & Tam, H. (2004). Machine fault diagnosis through an effective exact wavelet analysis. *Journal of Sound and Vibration*, *277*(4), 1005-1024.

Qing-Quan, J., Lian-Guang, L., & Yi-Han, Y. (2001). Abrupt change detection with wavelet for small current fault relaying. *PROCEEDINGS-CHINESE SOCIETY OF ELECTRICAL ENGINEERING*, *21*(10), 78-82.

Quek, S.-T., Wang, Q., Zhang, L., & Ang, K.-K. (2001). Sensitivity analysis of crack detection in beams by wavelet technique. *International journal of mechanical sciences*, *43*(12), 2899-2910.

Rao, K., Bhatnagar, A., & Misra, B. (2002). Laboratory investigations on rotary diamond drilling. *Geotechnical & Geological Engineering*, *20*(1), 1-16.

Rao, K. V., Murthy, B., & Rao, N. M. (2013). Cutting tool condition monitoring by analyzing surface roughness, work piece vibration and volume of metal removed for AISI 1040 steel in boring. *Measurement*, *46*(10), 4075-4084.

Ravindra, H., Srinivasa, Y., & Krishnamurthy, R. (1997). Acoustic emission for tool condition monitoring in metal cutting. *Wear*, *212*(1), 78-84.

Rowlands, D. (1974). Rock fracture by diamond drilling.

Salgado, D., & Alonso, F. (2007). An approach based on current and sound signals for in-process tool wear monitoring. *International Journal of Machine Tools and Manufacture, 47*(14), 2140-2152.

Samraj, A., Sayeed, S., Raja, J. E., Hossen, J., & Rahman, A. (2011). Dynamic clustering estimation of tool flank wear in turning process using SVD models of the emitted sound signals. *World Academy of Science, Engineering and Technology, 80*, 1322-1326.

Shah, L. D. F. A. (2015). *Wavelet Transform and Their Applications*: Birkhauser Boston.

Sheng, Y. (1996). Wavelet transform. *The transforms and applications handbook, 747*, 827.

Singh, G. K., & Sa'ad Ahmed, S. A. K. (2004). Vibration signal analysis using wavelet transform for isolation and identification of electrical faults in induction machine. *Electric Power Systems Research, 68*(2), 119-136. doi: http://dx.doi.org/10.1016/S0378-7796(03)00154-8

Strang, G. (1993). Wavelet transforms versus Fourier transforms. *Bulletin of the American Mathematical Society, 28*(2), 288-305.

Sun, Q., & Tang, Y. (2002). Singularity analysis using continuous wavelet transform for bearing fault diagnosis. *Mechanical Systems and Signal Processing, 16*(6), 1025-1041.

Sun, X. (1999). *A study of acoustic emission in drilling applications.* Paper presented at the The 37th US Symposium on Rock Mechanics: Rock mechanics for industry (USRMS), Vail, Colo, Rotterdam: Balkema.

Sung, C., Tai, H., & Chen, C. (2000). Locating defects of a gear system by the technique of wavelet transform. *Mechanism and machine theory, 35*(8), 1169-1182.

Takata, S., Ahn, J., Miki, M., Miyao, Y., & Sata, T. (1986). A sound monitoring system for fault detection of machine and machining states. *CIRP Annals-Manufacturing Technology, 35*(1), 289-292.

Tansel, I. N., Mekdeci, C., Rodriguez, O., & Uragun, B. (1993). Monitoring drill conditions with wavelet based encoding and neural networks. *International Journal of Machine Tools and Manufacture, 33*(4), 559-575.

Valens, C. (1999). A really friendly guide to wavelets. *ed. Clemens Valens*.

Vardhan, H., Adhikari, G., & Govinda Raj, M. (2009). Estimating rock properties using sound levels produced during drilling. *International Journal of Rock Mechanics and Mining Sciences, 46*(3), 604-612.

Wakuda, M., & Inasaki, I. (1991). *Detection of malfunctions in grinding processes.* Paper presented at the Proc 4th World Meeting on Acoustic Emission.

Wang, W., & McFadden, P. (1993). Application of the wavelet transform to gearbox vibration analysis.

Wang, W., & McFadden, P. (1995). Application of orthogonal wavelets to early gear damage detection. *Mechanical Systems and Signal Processing, 9*(5), 497-507.

Wang, W. Q., Ismail, F., & Golnaraghi, M. F. (2001). Assessment of gear damage monitoring techniques using vibration measurements. *Mechanical Systems and Signal Processing, 15*(5), 905-922.

Whittaker, J., & Miller Jr, A. (1991). Acoustic emission as a process monitor for diamond machining of metal optical components: Oak Ridge Y-12 Plant, TN (United States).

Wu, Y., & Du, R. (1996). Feature extraction and assessment using wavelet packets for monitoring of machining processes. *Mechanical Systems and Signal Processing, 10*(1), 29-53.

Xinzhou, D., Zhongxing, G., & Yaozhong, G. (1997). Application of wavelet transform in power system fault signal analysis. *Proc. CSEE, 17*(6).

Yesilyurt, I., & Ball, A. (1997). *Detection and severity assessment of bending fatigue failure in spur gear teeth using the continuous wavelet transform.* Paper presented at the VTT SYMPOSIUM.

Zhang, L., Li, Z., & Su, X. (2002). *Crack detection in beams by wavelet analysis.* Paper presented at the Third International Conference on Experimental Mechanics.

Zhu, K., San Wong, Y., & Hong, G. S. (2009). Wavelet analysis of sensor signals for tool condition monitoring: a review and some new results. *International Journal of Machine Tools and Manufacture, 49*(7), 537-553.

Zou, J., Chen, J., Pu, Y., & Zhong, P. (2002). On the wavelet time-frequency analysis algorithm in identification of a cracked rotor. *The Journal of Strain Analysis for Engineering Design, 37*(3), 239-246.